Revue des Composites et des Matériaux Avancés-Journal of Composite and Advanced Materials
Vol. 36, No. 1, February, 2026, pp. 107-124
Journal homepage: http://iieta.org/journals/rcma

Effect of Layer-Wise Fiber Orientation on the Mechanical Response of Laminated Composites: A Finite Element Simulation Approach

Haibat Lafta Gataa[1*], Ali Taha Mohammed[2], Ahmed Hashim Kareem[2], Diana Abd Alkareem Noori Kattab[3], Asaad Kadhim Eqal[2], Samir Ali Amin[4]

[1] Kut Technical Institute, Middle Technical University, Al-Kut 52001, Iraq
[2] Mechanical Techniques Department, Amarah Technical Institute, Southern Technical University, Basra 62001, Iraq
[3] Production Engineering and Metallurgy College, University of Technology- Iraq, Baghdad 10066, Iraq
[4] Department of Mechanical Power Techniques Engineering, Refrigeration and Air-conditioning, College of Technical Engineering, Al-Farahidi University, Baghdad 10001, Iraq

Corresponding Author Email: haibat-lafta@mtu.edu.iq

https://doi.org/10.18280/rcma.360111

Received: 8 December 2025
Revised: 5 February 2026
Accepted: 18 February 2026
Available online: 28 February 2026

Keywords:
fiber orientation, impact resistance, Cohesive Zone Modeling, damage tolerance, deformation behavior, interlaminar shear

ABSTRACT

The effect of fiber direction on the impact response is examined through detailed numerical simulations based on von Mises stress and deformation distributions for six-layer composite laminates. The three fiber layups (0°, 45°, 90°), (0°, 60°, 120°), and (0°, 75°, 150°) were studied with respect to stress intensity and deformation levels during simulated impact loading. The results indicate that peak von Mises stresses (83 MPa) occur at the outermost layers aligned with the impact direction, and that substantial term attenuation towards the outermost layers aligned with the impact direction, with stress attenuating to below 30 MPa through the inner layer, indicating an effective intra-layer stress distribution. The deformation response follows this trend, with the maximum displacement in the front layer of approximately 0.15 mm, decreasing to approximately 0.02 mm toward the back. Laminates with higher fiber orientation angles (0°, 75°, 150°) exhibit better crack blunting, owing to more widespread stress and less concentrated deformation. The results obtained in this paper are compared with the current literature, and the magnitudes of stress and deformation are in close agreement, thereby validating the predictive nature of the modeling methodology employed. This work underscores the importance of fiber-angle optimization in composite laminate design, particularly for balancing stiffness, impact resistance, and damage control.

1. INTRODUCTION

Composite materials are widely used in engineering projects due to their high strength-to-weight ratios, design versatility, and mechanical performance. Specifically, the aerospace, automotive, and defense sectors have significantly increased the use of fiber-reinforced composite materials, whose properties are vital to protection and damage tolerance. The geometrical structure of the fiber layers, as well as the fiber stacking sequence and orientation, has a crucial influence on a laminate's ability to absorb impact energy and suppress crack propagation. New methodological developments in numerical simulations (finite element and Extended Finite Element Method (XFEM)) have enabled the study of the complex interplay among fiber orientation, stress distribution, and damage evolution under impact loading.

In a study by Hu [1], Abaqus/Explicit finite-element analysis was used to study the impact resistance of composite laminates with varying fiber-layer orientations and hybrid fiber compositions. This paper revealed a strong correlation among impact velocity, residual velocity, and laminate orientation, and that laminates oriented between 0° and 45° exhibit the highest ballistic limit. Therefore, the authors concluded that placing Kevlar fibers at the rear of the structure and carbon fibers at the front significantly enhances energy absorption and penetration resistance. Wang et al. [2] provided an experimental and numerical study on CF/UHMWPE hybrid laminates against high-velocity projectiles (7.62 mm). Finite element analyses using an Enhanced Composite Damage Model showed that the layer sequence and fiber orientation are the key parameters that affect ballistic impact resistance. The data show that configurations with carbon fiber on the front and UHMWPE on the back exhibit the best energy-absorption characteristics and, at the same time, the lowest penetration depths. Du et al. [3] experimentally tested and simulated helicoidal laminates of carbon fiber fabrics by applying the impact testing and finite element to investigate mantis shrimp structures. The findings revealed that helicoidal fiber orientations were superior in energy absorption and delamination than those of quasi-isotropic laminates. It was found that a helicoidal angle of 12.8° yields the maximum impact resistance at low velocities, thereby maximizing the

biomimetic laminate architectures. Wang et al. [4] made a continuous-fiber helicoidal cylindrical polymer composite, which is reinforced by optical fiber through (3D) printing. They tested the product's dynamic behavior under high-strain-rate conditions using a Split Hopkinson Pressure Bar (SHPB). The resulting composites were observed to have significantly increased stress strength and toughness due to their 60° helical structure, which reduces the effects of porosity. Mechanical testing and numerical simulation showed that the use of optical fibers increased the maximum stress by 47% relative to unreinforced polylactic acid (PLA), highlighting the architecture's potential in the aerospace industry.

To investigate the ballistic impact on composite laminates made of sisal and glass fibers, Zelew et al. [5] conducted finite -element LS-DYNA simulations to determine how the composite reacts to the impact. Their analysis was on the impact of projectile velocity and orientation on residual velocity and damage distributions. The results revealed that the hybrid fiber system has greater energy-absorption capacity and deformation control, making it a viable option for future protective composite structures. Žmindák et al. [6] employed ANSYS to perform numerical simulations to determine the displacement, velocity, and energy-absorption characteristics of Carbon Fiber Reinforced Polymer (CFRP) and Glass Fiber Reinforced Polymer (GFRP) composites at different impact velocities. Their findings indicated that, in fibrous composites, fiber orientation significantly contributes to deformation and damage formation within the layered structure. It is worth noting that CFRP exhibited superior stiffness and impact performance compared with GFRP, thereby confirming ANSYS as a reliable predictive tool for impact simulation. In their numerical study based on finite element analysis, Banhart et al. [7] assessed the response of low-velocity impact on the oblique face of various fiber-reinforced polymer laminates, including carbon fiber-reinforced polymer (CFRP). In particular, their study shows that carbon-based composites are better energy absorbers and exhibit greater strength than glass and aramid under dynamic loads. Using sophisticated material modeling, the authors revealed the importance of stacking order and impact angles in the evolution of internal damage. The paper is critical in providing an important reference on the use of explicit-dynamics software for predicting failure in high-performance composite structures under complex impact conditions. Silva et al. [8] created an experimental testing and finite-element modeling study to explain the ballistic behavior of Kevlar 29 composite laminates. The experiment predicted the failure modes, dissipation paths, and perforation velocity (V°) of projectiles under STANAG-2920 conditions, and empirical experiments subsequently validated the simulation results. A close agreement between computational and experimental observations was observed, indicating the robustness of AUTODYN in predicting high-velocity damage in composite materials. Al-Akawi et al. [9] conducted experimental studies on the crushing behavior and energy absorption properties of glass-fiber/polyester composite tubular members as a function of fiber orientation angles (0°, 90°, 45°, and 60°). Their results show that fiber orientation significantly affects failure mechanisms and provide crash-worthiness parameters. Both tubes with 0°/90° fabricated orientation showed the highest specific energy absorption and the most favorable load-deformation behavior in axial compression. Xiao [10] proposed a combined modeling approach that incorporates the XFE and the Virtual Crack Closure Technique (VCCT) to model delamination in laminated composites. The single- and multiple-crack propagation behaviors were studied, and the numerical predictions were validated against experimental data. The evaluation of delamination paths using the XFEM/VCCT hybrid approach enabled prediction without predefined crack-growth trajectories. Yang et al. [11] reported a progressive damage finite element model consisting of three-dimensional criteria and cohesive zone elements to simulate low-speed impact on thermoplastic carbon-fiber laminates. Both numerical simulations and experimental measurements showed good agreement, with predicted errors less than 5%. Based on the study's results, the authors concluded that interlaminar delamination and fiber-matrix debonding are the dominant failure mechanisms under low-energy impact. Koetsier and Pavlovic [12] examined the use of embedded distributed optical fibers to quantify delamination crack growth in thick composite joints subjected to static and cyclic loading. The sensing methodology provided sub-millimetric spatial resolution of strain, thereby achieving a higher spatial resolution than conventional surface-based monitoring methods. Their results confirm that optical fiber sensing is a powerful method for structural health monitoring and for identifying hidden crack propagation. Alshoaibi and Fageehi [13] offer a critical review of recent developments in finite element modeling (FEM) of fatigue crack propagation, explaining its shift towards highly computational models and systems based on fracture mechanics. The authors review the critical strategies like Extended Finite Element Method (XFEM), Cohesive Zone Modeling (CZM), and Phase Field Modeling, whereby these approaches can be used to solve complex problems, such as crack branching and coalescence without constant meshing being required. Through the discussion of the issues concerning computational complexity and characterization of materials, the study provides information on how to choose effective numerical algorithms in various industries, such as aerospace and automotive engineering. In addition, the article suggests increased significance in applying experimental validation, including digital image correlation and 3D reconstruction, to improve the fidelity of predictive fatigue life simulations. Poojary and Hegde [14] conducted some experimental investigations to find the effect of fiber orientation angles on the dynamic behavior of pure carbon and carbon-Kevlar hybrid composites. The researchers conducted impact-hammer vibration tests and found that the natural frequency was optimized at 0° fiber orientation, whereas higher-angle orientations showed higher damping ratios. In addition, the experiment demonstrated that hybridization significantly increases energy storage and dissipation in the composites, thereby highlighting the synergistic interaction between carbon and Kevlar fibers. Dinesha [15] conducted a comprehensive literature review to evaluate the effects of fiber orientation and volume fraction on the impact resistance of natural fiber-reinforced biocomposites. The results showed that the optimal energy absorption performance was achieved with a combination of fiber orientation of 0°, 90°, and 45°, and fiber volume fraction of 30-50 percent. Furthermore, the sustainability advantages of natural fibers, such as flax, hemp, and jute, were highlighted. These are crucial, especially for structural components, where impact resilience is paramount.

Despite significant prior work on fiber angle and laminate response characteristics, research has mostly been limited to a few layers, single velocities, and/or simple material models. Such models do not always account for the interaction between

impact characteristics and the slow surface-propagation of cracks in layered composites. In addition, few studies have systematically validated finite element simulations of fiber-reinforced polymer (FRP) laminates against experimental stress–strain responses across a range of orientations and velocities. Thus, this research aims to address these shortcomings by developing and validating a detailed six-layer F.E. model. This mechanism would be investigated using this model to observe the effect of layer-wise fiber orientation on stress distribution, deformation response, and interlaminar energy flow under impact loading. The research aims to provide a more complete understanding of orientation-dependent stress redistribution and damage-tolerance mechanisms in laminated composites using this methodology, thereby offering valuable insights for the design of these lightweight, impact-resistant structures.

2. CRITICAL SYNTHESIS AND RESEARCH GAP

Recent advances in modeling and experimental approaches have addressed many aspects of hybrid architectures and damage evolution in fiber-reinforced laminates subjected to impact forces using FEM and XFEM of the grain structure [7-14]. Bonding between fiber layers plays a crucial role in bullet resistance and energy absorption, but prior studies have mostly focused on three- or four-layer setups. High-aspect-ratio multilayer systems are common in aerospace and defense composites, but little attention has been paid to this specific geometry. Moreover, although finite element damage models have been successful in simulating interlaminar delamination and crack propagation, single-impact or low-velocity validation has limited their use, leaving layer orientation and mixed-velocity effects largely unaddressed.

Although efforts to investigate fiber orientation have focused primarily on evaluating stress distribution and residual velocity, the understanding of interlayer stress transfer, a vital factor in energy dissipation and failure prevention in laminated composites, remains elusive. This work seeks to address this shortage by developing a six-layer finite-element model. A finite-element-based model will be applied to examine the effects of fiber orientation, bond strength, and impact velocity on the resulting stress distribution, deformation patterns, and interlaminar energy transfer across a wide range of impact velocities. In line with this, this robust simulation methodology emphasizes the damage tolerance, crack-arrest capacity, and energy-absorption efficiency of multilayered fiber layups. The subsequent work will aim to align numerical predictions with the current design principles governing the behavior of composite materials.

3. SECTION HEADINGS

3.1 Finite element modelling

The target plate is a square plate with six layers of the bullet fabric composite exposed, measuring 150 mm × 100 mm × 3 mm, and the properties of the bullet fabric are as indicated in Table 1.

The target plate is a square plate with six layers of the bullet fabric composite exposed, measuring 150 mm × 100 mm × 3 mm, and the properties of the bullet fabric are as indicated in Table 1. The thickness of the target layers is set to 0.5 mm each. Mesh convergence is studied in detail to determine the optimal finite element size. According to the experiment, 2 mm-sized elements are approaching the same residual velocity. Therefore, to ensure computational efficiency, a 2 mm element size is adopted in subsequent studies. The target plate had 89575 elements and 106338 nodes as the finite element model. The projectile is modeled as a three-dimensional solid element in the LSD-DYNA code. Figure 1 depicts a finite-element model of both the target and the projectile. To model the projectile, the impactor had a diameter of 12.7 mm and a cylinder height of 10 mm, and its properties are depicted in Table 2.

Table 1. Six plates composite material properties

Parameter	Value
Density	1323.3 kg/m^3
Young modules in a-direction, Ea	16115 MPa
Young modules in b-direction, Eb	16115 MPa
Young modules in c-direction, Ec	10323 MPa
Poisson's ratio, ba	0.2246
Poisson's ratio, ca	0.34472
Poisson's ratio, bc	0.34472
Shear modules, ab	5663.6 MPa
Shear modules, bc	2565.6 MPa
Shear modules, ca	2565.6 MPa
Longitudinal compressive strength, xc	144.19 MPa
Longitudinal tensile strength, xt	144.19 MPa
Transvers compressive strength b-axis, yc	40.2 MPa
Transvers tensile strength b-axis, yt	40.2 MPa
Shear strength ab plane, sc	32.16 MPa

Table 2. Impactor material properties

Parameter	Value
Density	7.2 E+5 kg/m^3
Young modules	2 E+5 MPa
Poisson's ratio	0.3
Bulk modules	1.66 E+11 Pa
Shear modules	1.66 E+10 Pa

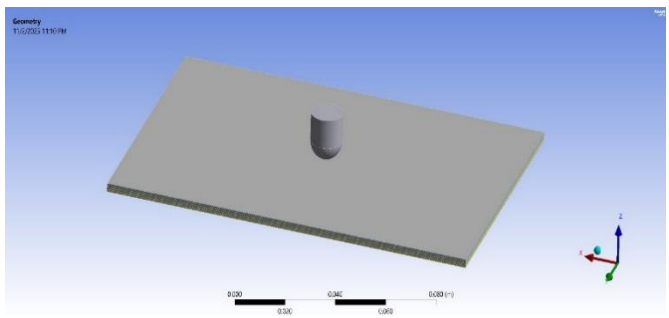

Figure 1. Projector and the 6-layer composite material design

3.2 Mesh independence test

Mesh independence tests are essential in ANSYS LS-DYNA simulations to ensure consistent results across varying mesh densities. The overall objective is to determine the optimal mesh density that maintains rendering efficiency while providing accurate results. A series of simulations with mesh sizes ranging from coarse to fine is performed to assess whether major changes in results occur as mesh quality improves. Mesh independence can be demonstrated by the stability of findings across mesh refinements with minimal

changes. A seven-mesh independence test was used in the simulation, with element sizes ranging from 0.5 mm to 3.5 mm in steps of 0.5 mm. In this type of testing, the mesh resolution is largely determined by the element size. The mesh components are more numerous for smaller items and fewer for larger ones [16]. The first measurement parameter identified during the test analysis was the deformation output. Table 3 shows the dependence of the test results on mesh element size. The deformation results indicated that information on the model mesh, including the number of elements and nodes, skewness, and orthogonality, was also presented in the table. When simulating in ANSYS, one should ensure the mesh is independent to ensure accurate, reliable results. The test should continue refining the grid network to determine whether values such as deformation remain constant as the grid becomes finer. They aim to determine the optimal mesh size, balancing computational speed and result accuracy.

Table 3. Simulation model mesh independence test

Element Size (mm)	Element No.	Nodes No.	Skewness	Orthogonality	Deformation (mm)
0.5	100600	118839	1	0.21	2.97
1	90800	107865	0.93	0. 63	3.36
1.5	89890	106754	0.88	0.83	3.73
2	89575	106338	0.79	1	3.93
2.5	89496	106225	0.77	0.95	3.92
3	89480	106200	0.76	0.91	4.26
3.5	89436	106130	0.67	0.88	4.61

In a laminated composite design, Skewness refers to the degree of angular deviation or asymmetry between successive fiber orientations within the laminate stacking sequence. Mathematically, it represents the non-uniform angular spacing between adjacent plies, which influences the anisotropy and directional coupling of in-plane stresses. A large skewness, as in a laminate with plies oriented at (0°, 75°, 150°), results in large angular errors between layers. These offsets create a web of multidirectional pathways for stress transfer and enhance shear coupling across different fiber orientations. As a result, the laminate has increased energy dissipation and a better ability to counter damage initiation and propagation. Low skew, as characterized by a design of (0°, 45°, 90°), is associated with almost equal angular separation between plies. This design encourages orthogonal interactions among the fibers, keeping stresses primarily constrained along the principal material planes and limiting multidirectional load sharing in the laminate. A 90-degree angular difference between fiber orientations is called orthogonality and determines the principal stiffness directions of the laminate, thereby influencing its mechanical behavior. This geometric connection determines the distribution of load-bearing capacity within the composite layers. In particular, orthogonality refers to fiber layers that are perpendicular to each other, i.e., 0° and 90°. These interleavings are beneficial for uniaxial stiffness and dimensional stability, at the same time, limit the laminate's ability to reallocate impact shear stresses. Highly orthotropic systems (e.g., (0°, 45°, 90°)) are typically characterized by dominant directional stiffness and are well suited for tensile or bending applications. Conversely, the less-orthogonal systems, such as (0°, 75°, 150°), exhibit oblique ply-to-ply coupling that enables gradual energy dissipation via shear deformation and stress rotation through the laminate thickness.

The results in Table 3 demonstrate that decreasing the mesh element size from 3.5 mm to 2 mm increases deformation linearly, from 4.61 mm (very coarse) to 3.93 mm (2 mm). With further fine-tuning of 1.5 mm, 1 mm, and 0.5 mm, there is no significant reduction in deformation: 3.73 mm (1.5 mm), 3.36 mm (1 mm), and 2.97 mm (0.5 mm). The deformation variation between the 2 mm mesh and the finer meshes (1.5 mm, 1 mm, 0.5 mm) is slight (when compared to the previous jumps), which means stabilization of the results. The skewness and orthogonality values are excellent at 2 mm (skewness 0.79, orthogonality 1.0), demonstrating a high-quality mesh, which is important for reliable finite-element analysis (FEA) results. At this point, the deformation results stabilize at 2 mm and are consistent with additional refinements; that is, the mesh is fine enough to represent the model's physics but not too expensive to compute. The finer meshes (1 mm, 0.5 mm) significantly increase the number of elements and nodes (and therefore computation time and memory consumption), but show only slight improvements in deformation prediction. The trade-off strongly supports the 2 mm mesh, which is relatively faster to compute and does not significantly affect accuracy. The 2 mm mesh also meets the recommended skewness (< 0.8) and orthogonality (> 0.7) criteria for good ANSYS mesh quality, which is another reason it was chosen. Figure 2 shows the six layers and the impactor model mesh.

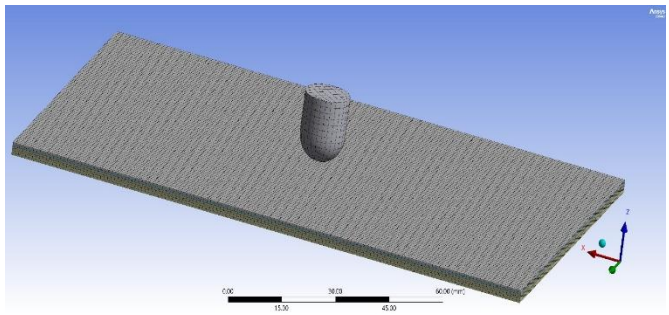

Figure 2. Six layers and the impactor model mesh

3.3 Modeling approaches

The modeling methodology is based on well-known rigid-body impact theory and its applicability in the LS-DYNA explicit solver. While rigid-body impact theory establishes the rules for momentum transfer, contact forces, and stress transfer during instantaneous impacts, LS-DYNA implements these rules via explicit time integration and contact algorithms, thereby solving for the continuous stress response within the composite target [17]. In this study, the impactor is idealized as a rigid body using the MAT_RIGID (MAT_020) material model in LS-DYNA, thereby eliminating projectile deformation during impact. This composite target interacts with the projectile using the AUTOMATIC_SURFACE_TO_SURFACE algorithm. The

algorithm tracks the contact surfaces that engage during high-speed contact. The upper composite layer, however, has a tangential resistance given by the dynamic friction coefficient $\mu = 0.3$ between the projectile and the upper composite layer. This value represents the actual interfacial states that form during impact loading, particularly at the fiber-matrix interface.

The Hertzian contact model is used to analyse the normal force between two surfaces. The local contact stiffness depends on the upper-layer elastic modulus of the composite. Classical rigid-body mechanics can be used to describe the contact mechanics of impacts, thereby enabling the correct determination of stress distributions and contact pressure [18]. This momentum-imbalance criterion is derived indirectly via the contact force (F) acting at the current time step, which determines the node velocities and displacements. Lastly, LS-DYNA decomposes the total kinetic energy (Ek) into elastic (Ee) and absorbed (Ea) components, thereby enabling explicit assessment of energy dissipation and recovery. Using explicit integration, the high-strain-rate response, along with the redistribution of interlaminar stresses and localized deformation of the composite laminate, is explicitly represented at every time step [19]. This unique process ensures the responsive incorporation of the analytical foundation of rigid-body impact theory into LS-DYNA's computational processes. In turn, this modeling paradigm bridges theory and numerical practice, thereby realistically modeling the interaction between the impactor and the multilayered composite laminate.

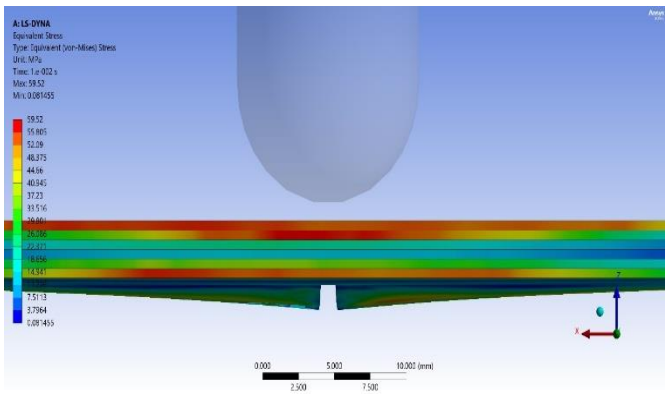

Figure 3. Impact on the composite plate of the stiff body (impactor)

3.4 Governing equations

Kinetic energy *Ek*(*t*), which will occur when an object with the mass m (impactor + weight) hits a composite plate at a velocity of v_0, which could be represented as follows:

$$E_k(t) = \frac{mv_0^2}{2} - \frac{m[v_i(t)]^2}{2} \tag{1}$$

The velocity relative to the impactor can be expressed using the following formula, where F is the experimentally measured force [20].

$$v_i(t) = v_o - \frac{1}{m}\int_0^t Fdt \tag{2}$$

The sum of the values of elastic energy Ee and absorbed energy E_a values is therefore the impact energy, which is produced in the composite plate, and therefore:

$$E_k(t) = E_e + E_a \tag{3}$$

The area of the elastic energy is the energy of the composite specimen in the form of rebound energy. The impact of the plate of the stiff body (impactor) on the composite plate is illustrated in Figure 3. At present, the equilibrium equation may take the form of:

$$\sigma_{ij,j}^t = \rho^t u_i + u^t \dot{u}_i \tag{4}$$

where, ρ^t and u^t are the density and dynamic friction coefficient of the composite plate at the (*t*) moment, respectively.

$$\sigma_{ij}^t n_j - \bar{T}_i^t = 0(onS_\sigma) \tag{5}$$

The stress boundary, which is denoted S_σ, enables the equivalent expression of the equilibrium equation and the load boundary condition to proceed as follows [21]:

$$\begin{aligned}&\int_V \delta u_i \left(\sigma_{ij,j}^t - \rho^t \ddot{u}_i - u^t \dot{u}_i\right) dv \\ &- \int_{S_\sigma} \delta u_i \left(\sigma_{ij}^t n_j - \bar{T}_i^t\right) ds = 0\end{aligned} \tag{6}$$

Since, under the impact load velocity, the composite goes through a geometric nonlinearity process, the strain-tensor, at time (*t*), may be expressed in the following form:

$$\varepsilon_{ij}^t = \frac{1}{2}\left(u_{i,j}^t + u_{j,i}^t + u_{k,i}^t u_{k,j}^t\right), (i,j,k = x,y,z) \tag{7}$$

Separate the equation given above into linear and nonlinear terms.

$$\varepsilon = \varepsilon_L + \varepsilon_{NL} \tag{8}$$

The following relationship in equation 9 represented the relation between σ^t_{ij} and ε^t_{kl} at the time.

$$\sigma_{ij}^t = \bar{\varrho}_{ijkl}^{t-\Delta t} + \varepsilon_{kl}^t \tag{9}$$

where, $\bar{\varrho}_{ijkl}^{t-\Delta t}$ resents the material elasticity matrix at the *t*-Δ*t* moment, and it can be obtained by coordinate transformation from the following equation:

$$\bar{\varrho}_{ijkl}^{t-\Delta t} = \lfloor T \rfloor \varrho^{t-\Delta t} [T]^t \tag{10}$$

3.5 Boundary conditions

The edges of the composite plate are fixed to prevent rigid-body motion during impact and to mimic the clamping in your Experiment. This permits local strain while preventing global translations/rotations, thereby enabling accurate stress and strain measurements. The projectile/impactor is modeled as a rigid cylinder (diameter = 12.7 mm, height = 10 mm) with material properties matching those of the experimental setup. In the simulation, the initial velocity in the Z direction (normal to the plate surface) or the impact load is applied, representing a drop or ballistic condition. The contact-friction multiple impactors ensure realistic interaction between the impactor

and the plate, with the simulation of frictional factors and energy transfer at the interface. The dynamic friction coefficient is introduced into the conservation and governing equations to ensure physical equivalence.

The model of the six-layer composite plate used a symmetric stacking sequence. The layers were grouped by their symmetry with respect to the midplane to construct a simpler model that still captures the physical properties. The six layers are divided into three groups; each group has the same orientation angle in the coordinate system. The first and last layers are grouped; the second and fifth layers are grouped more tightly; and the two middle layers are grouped even more tightly. (Layer 1 with Layer 6, Layer 2 with Layer 5, and Layer 3 with Layer 4). This design maintains stress and geometric symmetry across the laminate thickness and hence yields a net response similar to that of a balanced laminate. There were three orientation systems, coordinated as follows: System A [0, 45, 90, 90, 45, 0]: a conventional quasi-orthogonal layup used to study incremental shear transmission and the redistribution of normal stresses. System B [0, 60, 120, 120, 60, 0]: an oblique lay-up (suited to modelling helicoidal structures) that was designed to increase shear diffusion and delamination resistance. System C [0, 75, 150, 150, 75, 0]: a high-angle layup, which focuses on wide stress diffusion and improved impact energy attenuation. This allows simulation of the effect of fiber direction between layers on local stiffness, stress distribution, strain, and the affected cracked zone. Each layer has the Element Orientation loader, which allows the material property matrices to be appropriately transformed by the finite element solver to produce a specific fiber angle, resulting in a realistic anisotropic stress/strain response during impact.

4. RESULTS

The study of composite panels under various ballistic conditions is important for understanding their performance, as it enables simulations with varying fiber orientations to assess the effectiveness of fabric-oriented composite panels. To assess the impact of ballistics, projectile material, and size, and design and implementation of composite systems, a finite-element model was used. Within the framework of composite panels, precise mathematical and computational modeling, as well as the dynamic behavior of compounds, are also mandatory at various levels of the system [22]. Numerical studies on composite panels have been conducted, and several studies have reported on the high-velocity impact response of damaged panels [23, 24]. These experiments provide insight into the ballistic characteristics, energy absorption, and damage mechanisms of composite panels with varying orientation sequences.

4.1 System deformation (0°, 45°, 90°)

LS-DYNA simulations of a 6-layered ballistic impact composite with a stacking sequence of [0, 45, 90] depicted in Figure 4(a) and (b) provide an in-depth understanding of interactions between fiber orientation, interlaminar mechanics, and damage evolution in these high-velocity-loaded composites. The layers lie at 0°, which is essential for initial impact resistance, and the 0° orientation provides high in-plane stiffness and serves as the initial line of defense against projectiles. These layers absorb and retain most of the incident kinetic energy, thereby reducing penetration and increasing tensile and compressive strengths along their principal axes.

The adjacent 45° layers also provide oblique load paths; they redistribute shear stress, thereby reducing interlaminar shear forces, and direct energy into neighboring layers, thereby reducing the interfacial resistance across layers with different fiber orientations.

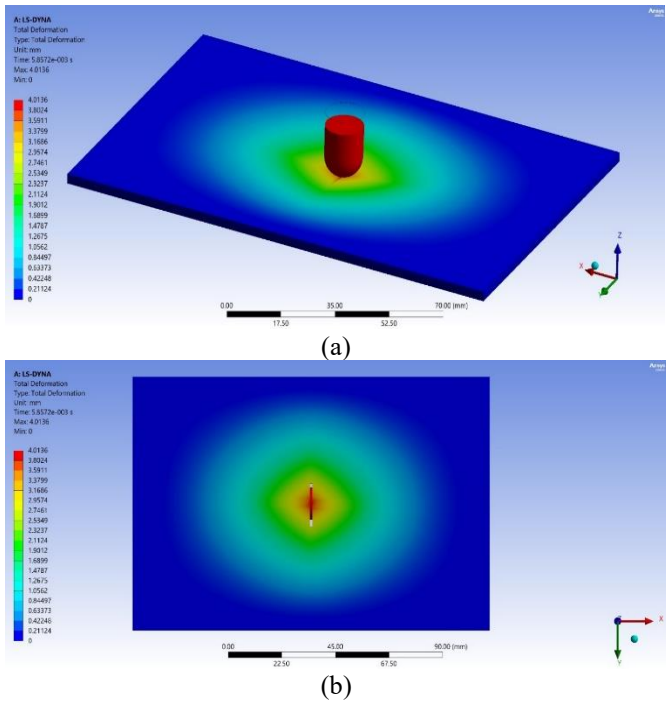

(a)

(b)

Figure 4. Six-layer system deformation (0°, 45°, 90°)

Central 90° layers, which are orthogonal to the main axis of impact, have a lower capacity to resist in-plane loads but a high capacity to absorb through-thickness stresses. Their positional arrangement focuses matrix cracking and fiber-matrix debonding at the impactor area, where maximum deformation is observed, as revealed by the FEA contour plots, with values up to 4 mm. The gradual change in fiber direction across the laminate thickness provides fine-tuning of local stiffness, resulting in a controlled deformation gradient and a strong interlayer stress-transfer mechanism. This anisotropic architecture will support several redundancy plans to reduce failure: (1) a gradual debonding process under the influence of the energy-sliding slabs; (2) the alternate lay-up to block the multiaxial crack pathways; and (3) a gradual radial strain dissipation outside the ballistic impact zone, which demonstrates the ability of stiffness and ductility to work synergistically.

In dynamic impact simulations, the computational model uses a refined mesh that deliberately captures these phenomena without the prohibitive computational costs required to obtain stable results on high-resolution models. These observations are supported by numerical experiments focusing on this laminate structure, which suggest in addition that the combination of 90 o layers with 0 o and 45 o layers produces the best balance of ballistic limit, energy absorption, and crack arrest; fiber orientation transitions are the main factor in determining interlaminar delamination and fiber failure. In conclusion, the visual and computational results show that, for maximizing impact energy dissipation in rapidly loaded laminates, intelligent fiber organization and fiber

rotation in thick-section composite materials are key [25].

Figure 5 presents the quantitative distribution of deformation suffered by all six layers in a composite laminate when impacted by bullets with increasing velocity levels, corresponding to one particular fibrous orientation itemized by [0°, 45°, 90°, 90°, 45°, 0°] in lay-up sequence. The X-axis represents spatial position along the panel width, and the Y-axis shows the localized deformation amplitude at each layer, enabling direct comparison between outer and inner layers. In this display, impact energy propagates through the layers stacked in sequence, like water recycling: the surface-against-impactor first layer shows sharp maximum deformation peaks and a maximum localized value at a single point; subsequent layers act successively less strongly (with an ever more superficial emphasis). Layers laid at 45° or 90° exhibit distinct intermediate responses, underscoring the roles of stiffness anisotropy and interlayer shear in redistributing forces and inhibiting delamination. The sixth and final layer, located at the rear of this test specimen, showed the lowest deformation at its center. This evidence clearly indicates that the system suffers from a limitation in its ability to convert point-like, high-impact forces into distributed, multilayer energy absorption. In plotting all six-layer responses, this graph represents the dynamic interplay between fiber direction, stacking order, load-bearing capacity, and protective value [26].

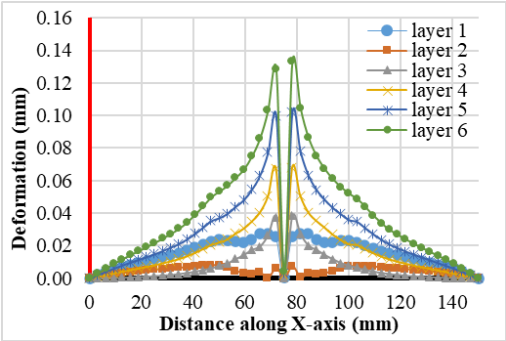

Figure 5. Quantitative distribution of six layers (0°,45°,90°) system deformation

Layers 1 and 6 show the deformation profiles, which were constructed initially as a series of layers and subsequently from the overall deformation contours. In the first layer which faces directly with an impact of extreme force, deformation soars to 0.145 mm at the center of impact, then symmetric save for two fall-offs: one to 0.09 mm at X = 60 mm and X = 92 mm; another down 0.05 mm at both X = 40 mm and X = 120 mm; and finally, it is almost nonexistent along the panel's edges (less than 0.01mm maximum). This sudden central peak suggests that the first layer, being stiff along the fibers yet absorbing the brunt of impact, is most susceptible to fiber micro-buckling, shear-induced debonding, and possibly matrix cracking. Interlaminar shear and staggering the inner 45° and 90° of each layer effectively dissipate energy; they reflect energy at the film/fiber and interface interfaces. By the time the force reaches the rear sixth layer, the deformation profile has changed significantly. The maximum peak now lies at about 0.027 mm (frontal conditions were more than 80% higher). This curve has a two-lobed shape, 0.022 mm in whale bone fashion, at X = 60 and 92 mm, and also broadens toward the edges, with residual values less than 0.005 mm past X = 40 mm and X = 120 mm. The characteristic peaks in this profile are evidence of energy having been absorbed, scattered, and delocalized by the multidirectional fibers with a large number of delamination arrest events, which is one of the characteristics of highly effective ballistic composites in the stacking process that must not be missed. In the total contour plot, the entire laminate experiences a maximum overall out-of-plane deformation of only 4.01 mm, even under severe impact; all layers work together to prevent collapse or hole formation. There is a low-to-high transition in both types of progressive improvement from frontal emergency kind to rear-body thoroughgoing treatment, as to whether [0/45/90/90/45/0] layup in ballistic resistance is feasible through literature indicating that in fact from industriously analyzed theoretical predictions and experiments today recorded data it acts on impact attempt locally so as broadly benefiting strength left behind while at once minimizing risks from failure [27].

Meanwhile, layers 2 and 5 of this are critical transition layers located at respective 45° between exterior faces (0°) and the mid (90°) core. They have a profound impact on the deformation that expands and disperses from the initial point of ballistic impact, the center of deformation of layer 2. The highest deformation value is approximately 0.022 mm at X = 76 mm, as shown in the provided deformation chart. It declines rapidly from the peak of the curve; at X = 60 mm and X = 92 mm, the value is approximately 0.013 mm; at X = 40 mm and X = 120 mm, it drops below 0.007 mm. Perhaps more dramatically, center of deformation for the fifth barrier layer crests at about 0.059 mm, significantly greater than for layer two but suggesting more energy transfer through deeper layers as the wave reflects and refracts fiber angle in various ways; at X = 60 mm and X = 92 mm, the value is approximately 0.037 mm before dropping to under 0.015 mm towards edges. What causes this difference is that layer 2, closer to the imparter of shock impact and shielded by the harsh 0° veneer, but shielded from off-axis stress/shifting along its natural transverse direction by middle fibers in a stack, where there is no other way for shear forces (shear) to dissipate at once like this quickly, can theoretically deduce energy roughly equivalent. Meanwhile, layer 5 is subject to greater cumulative redistribution of load because it directly interacts with waves from the layers above at 90°; this dispersion of energy further reduces the sharp deformation peaks. From beginning to end (center) for layer one, peak deformation is 0.14 mm, then decreases to below 0.01 mm at the margins between layers; meanwhile, layer six at the center has deformation of approximately 0.027 mm. This sophisticated composite material is heatproof, soundproof, and ballistic-resistant.

Layers 3 and 4 form a 90° angle, oriented in this configuration. The samples exhibit low but widely distributed deformation values; the morphological changes under ballistic impact highlight the importance of bridging mechanisms and enable redistribution of transverse fiber tension across the remainder of the surface. Regarding the deformation map, the highest values for both Layer 3 and Layer 4 occur at the specimen center (X ≈ 75 mm), with deformation values of 0.014 mm. In contrast, at X = 60 mm and X = 90 mm, the deformation value reduces to about 0.008 mm due to crack initiation in peripheral regions outside the impact loci (X = -40 mm and X = 110 mm). The deformation further decreases in these outer layers, often reaching a value below 0.003 mm. This low-deformation property results from the orthogonal positioning of the layers: these zones do not transmit energy along directionally oriented (X-axis) strains but dissipate

energy through transversely spanning forces, primarily through mechanisms of matrix and interfacial strain. This behaviour plays a key role in stopping crack propagation and reducing the impact energy of lateral forces. The similar behaviour at Layers 3 and 4 can be explained by their symmetric positioning relative to the mid-plane, which maximizes mechanical responses of equal magnitude. This has been conceived as a design principle for intuitive implementation in public buildings and bridges: avoiding in-phase buckling of layers not only provides greater continuity to the load path but also reduces, at random, any rebalancing errors that had previously been expected. By comparison, 0° (first layer) hits a maximum of around 0.14 mm; then, in sharp contrast, 0° again (Layer 6 at back) falls abruptly to about 0.027 mm. This clearly shows that the inner 90° layer can reduce the peak stresses, should there be no alternative for an object or surface to bear the force, and it also plays a key role in distributing the energy load across the laminate. These results fully corroborate the theoretical prediction and simulation analysis reported elsewhere in the latter study, which show that placing a 90° layer at the center provides an energy-damping mechanism that prevents cracks from propagating into it. In contrast, none of the other four can emulate this.

4.2 Von Mises equivalent stress distribution (0°, 45°, 90°)

As shown in Figure 6(a) and (b), (von Mises) equivalent stress distribution for the six-layer composite system [0°, 45°, 90°, 90°, 45°, 0°], damage and stress waves travel at the primary three layers since fiber anisotropy, stacking sequence, and local dynamic load aggregation lamina, evident also from partial wave energy absorption.

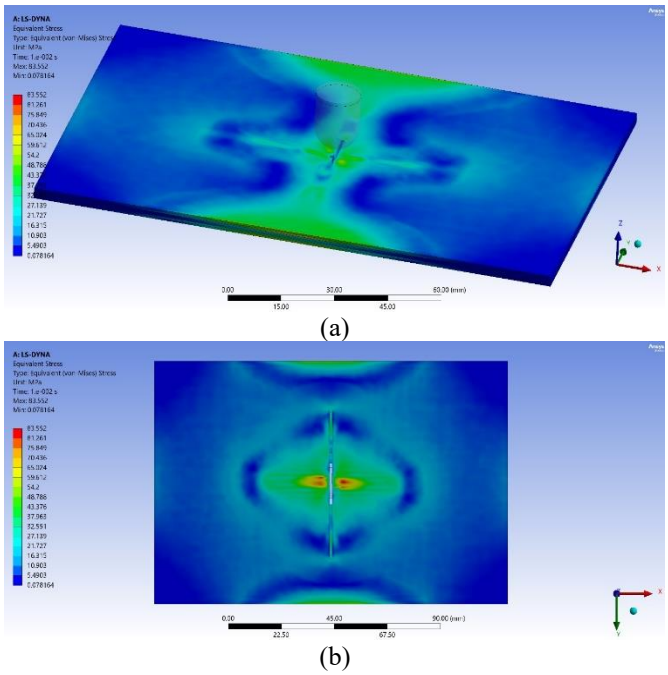

(a)

(b)

Figure 6. (Von mises) equivalent stress distribution for the six-layer [0°, 45°, 90°] composite system

After the impact, stress is most concentrated directly beneath the point of impact and reaches a peak of about 83.6 MPa, with steep gradients radiating outwards; interlayer interface stressing along oblique planes inwards and laterally; these regions signify where maximum energy dissipation occurs to drive filling or between lamina (matrix cracking) and ultimately opening up a hole. The front 0° layer takes the brunt of the impact: having little in-plane elasticity itself, it is subject to the highest stresses in this area and, together with its fiber principal direction, serves as a vector for stress redistribution. The stress contours indicate that, being nearest to 45°, with the next pair on either side acting as a "bridge" between layers, off-axis shearing is suppressed at these sites and shifted toward neighboring ones. This action not only helps arterialize cracks but also shifts compressive loading to tensile loading on planes with moderate stress values of 27 to 45 MPa. The 90° layers deeper inside display broader stress zones of much lower magnitude – generally under 20 MPa in the center and falling near the edges - because, undoubtedly, for much of this through-thickness direction, their in-plane rigidity balances such tendencies quite well. This protects the underlying layers and minimizes direct stress transfer; as a result, the penetration risk is reduced, and energy can be absorbed by deformation at both the matrix and interface levels without compromising the system. Quantitatively, the respective deformation values for comparison are as shown in this table: the first 0° layer is between 0.14 and 0.145 mm there sink to less than 0.01 mm sixth (rear) 0° layer after full energy absorption has ceased currently stands at about 0.027 mm, representing a drop of 80% and supporting the stress distribution maps The results, supported by the finite element and experimental methodology given in research articles, point to a stacking sequence tailored for incident impacts converting energy into peak localized stresses combined with widely distributed deformations which is just what is needed in impact resistance systems, penetration can be minimized no helical or whirlpool shaped breaks propagated through several layers, since there are many layers orientations where stress suppression occurs quantitatively [28].

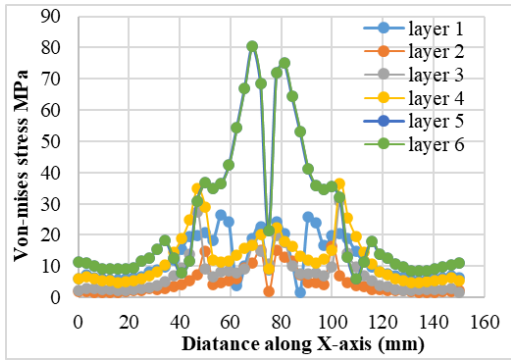

Figure 7. (Von mises) equivalent stress distribution along the X-axis for the six-layer composite system.

Figure 7 shows the von Mises stress distributions in the individual layers of a [0°, 45°, 90°, 90°, 45°, 0°] composite laminate subjected to ballistic loading. The X-axis shows the lateral position over the panel's area map. In contrast, the Y-axis shows the stress of each laminate in MPa, with oriented layers indicated and both comparison points. At the same time, this visualization makes clear how the particular stacking sequence of layers separates each layer through stress transmission. The experimental plate X-axis is shown in this chart, with multiple positions along the 90° axis, 45°, and elsewhere. The stress response in each layer is strongly dependent on its position and alignment, with maxima exceeding 80 MPa in the rear layers and falling below 35 MPa even in deep-lying 90°-oriented layers. The stepped peaks in a

number of these curves also reflect interlaminate effects and energy transmission from the impact site. Incoming and outgoing stress waves are coupled and redistributed across the layers.

Layers 1 and 6 in Figure 7 show how the von Mises stress for the [0°, 45°, 90°] composite varies along its X-axis, providing a detailed quantitative view of how the 0° oriented surface layers respond to the strike of an impactor and, in an adept manner, in which stress is regularly given up through thickness. In the first layer, which is in direct contact with the projectile, maximum von Mises stress at middle (X = 75 mm) reaches nearly 81 MPa, with lesser local peaks of about 34 MPa at X = 55 mm and X = 95 mm, a stress plateau between 10-14 MPa beyond X = 40 mm and X = 110 mm where stress fields widen out side to side. This sharp central maximum reveals the localization of impact-induced loads in stark relief. By contrast, the sixth (bottom) layer exhibits a much more modest and spread-out stress response, with central von Mises stress peaking at about 28 MPa at X = 75 and falling off to 13-15 MPa in the same local-secondary peaks, while remaining about 10 MPa elsewhere. This sudden dip indicates that stress has dissipated rapidly horizontally and spread widely through all the intermediate 45° and 90° laminates, so multiple interfaces absorb impact energy. Consequently, the back layer is never subjected to catastrophic collapse due to local overstress [29].

The von Mises stress distributions of the second and fifth 45° oriented layers are shown in layers 2 and 5 in Figure 7. As shown in Figure 7, they are important for transitional energy-dissipation zones in a [0°, 45°, 90°] composite system under rapidly increasing forces or impulses. A moderate but widespread peak stress envelops the stress profile of the second layer X ≈ 78 mm: the greatest central value is 15.2 MPa and additionally amongst local peaks there are 14.7 MPa off lateral top-post consumes at about X ≈ 51 mm and 16.5 MPa top-side offset center respectively; furthest away from these volcanic areas stress quickly drops off to 4 and 5 MPa and drops down to 2 MPa at the edge along X-axis. This relatively low wave pattern reflects that the best path for off-axis shear transfer is ruled mostly by directional crack growth (although cracks are constrained to remain quite short in this case). They are quickly suppressed by the 90° and 0° interfaces, where they meet them on both sides, because the first layer around that time becomes thicker for a short span, after which the layer ceases to thicken further. In the rear surface layers, the fifth-layer stress levels show a peak of 81.2 MPa at X ≈ 78 mm and a secondary peak of 73.7 MPa at X ≈ 97 mm, between which are shoulders at 34 – 36 MPa (X ≈ 62, 100 mm). Moreover, the drop from a level far from the edge to 14 MPa at the edges on either side of the centerline indicates that these high stresses are at their maximum. As waves guided by hardness waves traveling up from the sixth layer (rear 0° layer) touch it, the fifth layer transiently staggers longer before allowing itself to be dispersed. This phenomenon is characterized by sub-surface crack branching in closely spaced areas and impending interlaminar crippling. Stress results on the 45° layers, as opposed to the first 0° layer (top of peak ≈ 16.6 MPa) and the rear 0° layer, show that the stacking sequence leads to impact energy being directed into oblique, dissipative tracks, which keep face contact openings and promote multilayer edging of cracks [30].

When the stress distribution curves for the third and fourth layers in Figure 7 composites (both with 90° fiber orientation) are plotted, it becomes clear that in the [0°, 45°, 90°] direction, the middle laminates act as primary barriers for cracks at layer interfaces. The Layer 3 stress distribution curve shows stress peaks at 35 MPa (X ≈ 46 mm) and 106 mm, with the latter peak (22 MPa) being lower. There is also a bell-shaped area above the centerline, with a 14 MPa stress wave at y ≈ 76 mm; the stress decreases to 5 MPa along the edges of the plates. For the fourth layer, its behavior follows the same pattern as that of the third layer. Spin in these middle layers. Layer 5 has an approximate maximum von Mises stress of 27 MPa at X ≈ 49 mm, and another peak at around 22-23 MPa at X 101 mm. This kind of profile represents efficient absorption and dispersion of energy load. The behavior in these 90° layers contrasts sharply with that in the first and last 0° layers, where the front layers receive peak stresses of 16 MPa (approximately at the center) and the rearmost layers exhibit the highest impulse histories (roughly 80 MPa peak). This contrast underscores how much the effects of energy transfer differ with cross-layer orientation. In the third and fourth layers, the smooth, well-spread valleys and lack of a conspicuous central peak suggest effective crack retardation and thus early energy dissipation.

4.3 System deformation (0°, 60°, 120°)

Figure 8(a) and (b) illustrates the deformation patterns in ballistic impact on a six-layer composite with alternating (0°, 60°, 120°, 120°, 60°, 0°) fiber orientations. The first layer (0° impact) exhibits the highest central deformation in the ring, at approximately 4.38 mm, which declines rapidly to 1.48 mm as the radial distance from the center approaches 25 mm. The peak deformation was approximately 1.38 mm for the second (60°) layer and 0.79 mm for the fifth layer, with a symmetric distribution across the width. These intermediate values again confirm the effectiveness of oblique orientation in preventing crack penetration, offsetting shock, and producing ductile shear spread. The third and fourth layers (120°) show maximum deformations of around 1.08 mm and 0.98 mm, while strain fields are broad enough to cover nearly 0.8 mm.

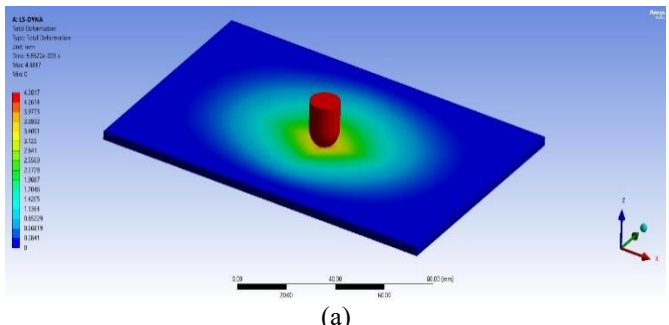

(a)

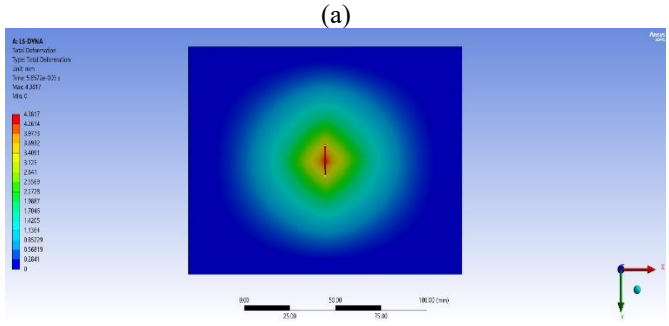

(b)

Figure 8. Six-layer system deformation (0°, 60°, 120°)

Under these conditions, crack arrest in the plane remains good, and load redistribution across multiple directions remains debated. The surface layer at 0° is significantly lower,

with a maximum deformation of 0.09 mm; the periphery is virtually intact. The pattern of deformation indicates that the maximum displacement occurs at the point of impact, and energy dissipation is evenly distributed across layers whose angles are staggered, thereby supporting the principle of optimal design in composite armor. The deformation profiles for all six layers are shown in Figure 9. The X-axis denotes the location within the specimen width, and the Y-axis denotes the local deformation magnitude of each layer; hence, it is straightforward to compare the attenuation and distribution of strain across the thickness. Such multiphase mapping also shows an even more pronounced progressive decay in peak deformation. The surface layer, with the highest deformation (approximately 0.135 mm), gradually transfers the load to the next layer, which has a smaller peak, as impact energy is dissipated, reallocated, and reduced by oblique and alternating fiber orientations. The intricate action of the 60° and 120°layer curves again demonstrates the importance of layer angle in load spreading, which results in more extensive, multi-peaked deformation patterns [31].

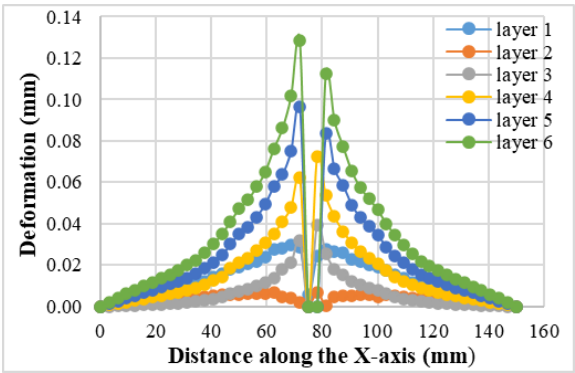

Figure 9. Quantitative distribution of six layers (0°, 60°, 120°) system deformation

The fact that the lower layers are symmetrical and that the laminate was symmetrical supports the symmetry of the lower layers. It demonstrates that there was desirable residual protection after delamination. The low deformation also indicates multiple directional load sharing. Overall, this chart summarizes the strike-blunting and crack-trapping behaviors observed with the [0°, 60°, 120°] system and fully confirms this novel layer sequence for ballistic applications of advanced composites in impact damage. The deformation distributions in layers 1 and 6 in Figure 9, corresponding to the first and sixth layers (both with 0° fiber orientation), vividly show the redistribution of impact energy and the development of cracks from the strike face to the rear surface. In the first layer, the central stresses bearing down on it are those experienced by the impactor itself; the peak deformation reaches 0.135 mm at X ≈ 76 mm. Dual maxima at X ≈ 65 mm and X ≈ 90 mm, just below 0.13 mm, then symmetric decline below 0.03 mm at the plate edges. This indicates that a great strain has been concentrated there by one-sided compression, and that, before long, rapid cracking will occur at its decelerating center. As the load propagates through oblique layers, interlaminar interfaces scatter and dissipate energy: successive layers exhibit deformation peaks that decrease to 0.032 mm for the rear (sixth layer), where broad lateral plateaus at X = 65–90 mm reach only 0.025 mm, and edge values drop below 0.005 mm. This pattern demonstrates a strong, multi-directional wave and a crack-blunting phenomenon: slight microcracks in the matrix and delamination between layers grow into initial cracks at the impactor site. The second and fifth layer in Figure 9, arranged in a direction of 60°, seems far more necessary for distributing energy from an impact along the x-axis layer and controlling crack growth than any combined resistance it manages between shear within itself and transfer to neighboring laminae. The deformation profile for the second layer displays that at around X = 76 mm, there is a maximum deformation of roughly about 0.0068 mm, with two plateaus of high value nearby on either side (> 0.0063~0.0064 mm at X ≈ 65-75 and 90 mm) and then 0.002 mm extending slightly to the region. The fifth-layer peak deformation (0.0067 mm) decreases on both sides and does not increase beyond this position.

Layers 3 and 4 in Figure 9 illustrate the advantages of delayer-stacked layers oriented obliquely. The deformation in the third layer was 0.039 mm at X ≈ 79 mm; a deformation peak of 0.032 mm was observed at X ≈ 68 mm; the deformation then gradually decreased symmetrically, reaching zero at X ≈ 40 mm due to the crack opening. The fourth layer has a very similar shape to this profile. A maximum deformation magnitude was 0.031 mm and uniformly distributed midsection, averaging about 0.025-0.028 mm, then dropping to 0.006 mm at the ends of a specimen. The composite sticks to amplify this principle: some of the energy is absorbed, and parts are broken off in 120° layers along the X-axis. Here, new cracks have to bend around or impinge on the fiber-matrix interface. The fact that the deformation curves are more consolidated and less saw toothed indicates that layer orientation and configuration are closely related to the undoing of sharp-interface debonding events, such as general inelastic yielding of the matrix or small, blind deductions, as these intermediate cracks propagate.

4.4 Von Mises equivalent stress distribution (0°, 60°, 120°)

A six-layer composite exhibits a much more complex pattern in how the stacking sequence and layer orientation transfer ballistic impact stresses from the surface to the layer depth. Figure 10(a) and (b) shows that through the entire set of layers, maximal stress is experienced at ≈66 MPa just under the impactor contact.

The bright yellow-red areas in Figure 10 are evident. With a significant gradient toward the sides, where stress decreases below 8 MPa close to the plate edges. A 60° and 120° layer shows characteristic stress patterns with two well-distributed peaks, one for each direction of x-axis loading, resulting from shear transfer between layers. This fact indicates that the central layers of the structure (especially the 120° layers) can be exposed to stress maxima ranging from 32−44 MPa, whereas stress peaks are measured around 36−66 MPa at the second and fifth layers over 60°, which dampen quickly at the boundaries.

These moderate discrepancies support the experimental study [32], which highlighted that angled layers do not directly transfer impact load to the rear face but dissipate energy through shear, friction, and fiber-matrix interlocking mechanisms, thereby mitigating through-thickness cracks and delaminations. The most desired benefit is the minimum stress in the rear surface (below 10 MPa out of the direct impact path), which demonstrates that the hybrid [0°, 60°, 120°] stacking configuration effectively converts localized loading to broad, multi-directional stresses field, promoting both energy dissipation and post-damage performance (residual

strength), whereas observed X patterns support strong crack blunting and dispersed damage propagation across the composite.

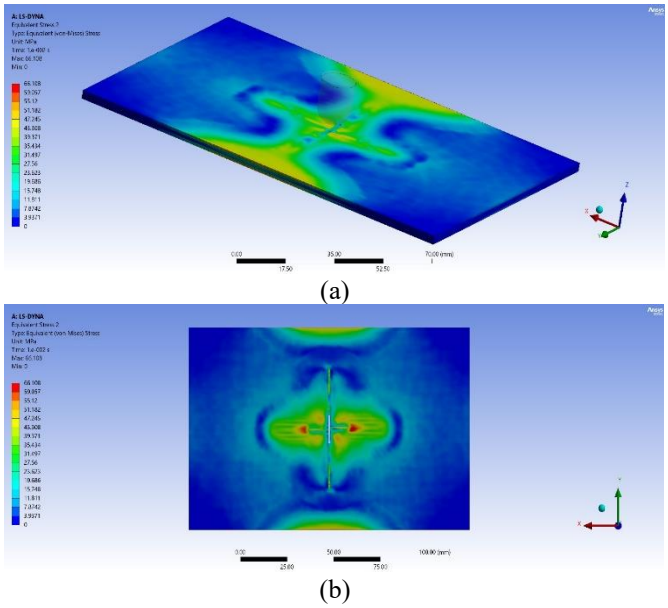

Figure 10. (Von mises) equivalent stress distribution for the six-layer [0°, 60°, 120°] composite system

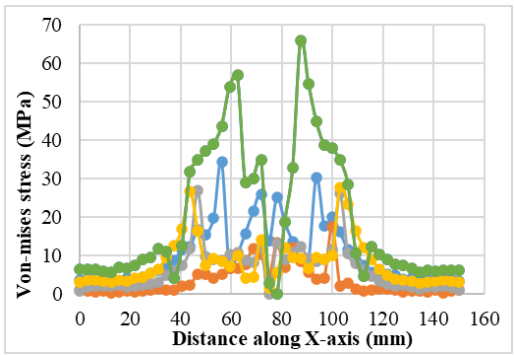

Figure 11. (Von mises) equivalent stress distribution along the X-axis for the (0°, 60°, 120°) six-layer composite system

Layer stress attenuation and layer responses under ballistic loading for (0°, 60°, 120°) composite, based on von Mises stress distributions for all six layers, are presented in Figure 11. The lateral spatial position is denoted on the X-axis, while the Y-axis shows the local von Mises stress (MPa) for each layer across the width, allowing for in-plane and through-thickness stress transfer at the layer level. The data suggest the outermost (0°) rear layer creates the highest peak (over 66 MPa), with wide stress plateaus and gradients; however, internal layers at 60° and 120° produce lower, multimodal peaks (15–36 MPa for 60°, 9–25 MPa for 120°) that broaden and propagate the incident stress by x-axis shear. Symmetry between the second/fifth curves and the third/fourth curves confirms stable, symmetric energy dispersion signifying balanced stacking. The differences in individual-layer responses clearly reveal the role of fiber orientation: stresses localize and propagate in patterns determined by the layer angle, and the multilayer structure ensures that both direct perforation and severe through-thickness cracking are avoided. This broad, multi-layer perspective illustrates the [0°, 60°, 120°] system's efficacy in mitigating and attenuating peak and residual impact stress.

Layers 1 and 6 in Figure 11 show the von Mises stress distributions for the first and sixth 0° oriented layers in the (0°, 60°, 120°) composite, respectively, suggesting that the outer laminates failure levels are sequential, absorbing/losing impact energy as the layers sequentially deform and dissipate energy which shapes the multi-axial stress environment using numbers as the qualitative indicators of success in protection. The peak stress approaches 66 MPa at X ≈ 92 mm, with short, but more localized, stress excess 55 MPa found at X ≈ 62 mm and X ≈ 111 mm, and a broad shoulder of 35–45 MPa across X ≈ 50–120 mm and below 8 MPa at the edges of the specimen; this sharp, multimodal loading profile suggests the violation of both fiber and matrix failure modes and the imminent formation of microcracks or shear bands at the principal impact site. In the backmost sixth layer, the stress gradient is particularly diminished, with the von Mises maximum at ~35 MPa at the center and lower side peaks in the 20–30 MPa range, before dropping to a near-constant 5–10 MPa along the mid-distal borders. This reduction in penetration indicates how effective the laminate is at diffusing and capturing stress through a structure of inclined layers that can generate in-plane forces, contribute to partial delamination, and encourage fiber bridging, thereby inhibiting the transmission of vital stress across the thickness. The outer 0° faces exhibit high stress magnitudes (> 80 MPa) and a pronounced shear-induced effect with increasing layer angle, whereas the central 120° layers further blunt through-thickness transmission relative to the second and fifth 60° layers (which have secondary maxima of 36–66 MPa). This layered attenuation mechanism prevents cracks at the maxima of stress from penetrating the rear face due to mismatches in mechanical impedance and multilayer friction.

The von Mises stress profiles of the 2nd and 5th 60°-oriented layers, shown in Figure 11 (layer 2 and 5 curves), illustrate how angled layers serve as a key transition threshold between peak and dispersive stresses induced by ballistic impact. The stress profile in the second layer shows a maximum of ~35 MPa at X ≈ 59 mm (~1.6 mm below the impact surface), flanked by local peaks of 36 MPa at X ≈ 94 mm and moderate shoulders of 24–30 MPa across the main impact zone (X ≈ 50–100 mm), with the wings decaying rapidly to 3–7 MPa near the edges of the sample. The profile of the fifth layer is also more complex and multimodal, with a narrow main peak of 66 MPa at X ≈ = 93 mm, secondary peaks at X ≈ = 62 mm around 57 MPa, and broad shoulders (~32–44 MPa) that are approximately symmetrical across the plate and then gradually fade below 12 MPa beyond X = 120 mm. The evolution of this pattern reflects both the propagating and slowing down functions of intermediate layers. The 60° layers have a strong ability to convert a pulse into shear and to resist direct stress transfer.

The third and fourth 120°-oriented layers in Figure 11 show that deep, angle-oriented layers are critical for energy dissipation and fracture [9]. In the third layer, the most pronounced features include the peaks of 27 MPa at X ≈ 45 mm and 26 MPa at X ≈ 105 mm, with a broad, multimodal population of intermediate stress state in the 8–13 MPa range across the width of the specimen, low values near 0 MPa (X ≈ 76 mm), and an edge baseline of approximately 2 MPa. The fourth layer is similar to that, with almost identical edge-to-edge behavior: main stress maxima 27 MPa at X ≈ 45 mm, 26 MPa at X ≈ 105 mm, broad internal plateaus 8–14 MPa, and lower edge values (2 MPa). With stress values (up to 66 MPa)

recorded in the outermost 0° layers being substantially higher than these relatively modest, distributed peaks, the 120° layers primarily appear to be focused on absorbing, distributing, and blunting the stress pulses; stress pulses are primarily dissipated via damping shear stress and bulk local matrix yielding rather than through-thickness attenuation. Such a pattern serves to confirm crack arrest at the interior and energy dissipation from the crack process zone.

4.5 System deformation (0°, 75°, 150°)

The six-layer composite system of (0°, 75°, 150°) and its deformation distribution results are shown in color-mapped and three-dimensional field contour images in Figure 12(a) and (b), respectively, demonstrating that adequate angular stacking achieves efficient stress mitigation with minimal damage, resulting in a maximized impact. Maximum deformation at the impactor site (middle) is on the order of 4.36 mm at the surface and falls radially: 20 mm from the center, max displacement marginally reaches 3.16 mm; 40 mm reaches 0.016 m but only 0.02 mm out (70 mm max displacement), then approaches zero by the plate bounds. Layer assessment shows that nearly all the local impact energy is absorbed within the top 0° layer (3.5–4.4 mm at the center); subsequent 75° and 150° layers then sequentially limit the peak center deflections to roughly 2.7–3.4 mm and 1.6–2.3 mm, respectively. Deformations in the central layers (150°) stay primarily below 2 mm, whereas the last rear layer (0°) displays displacement maxima under 1 mm, showing through-thickness reduction of nearly 85% from entry to exit face. The reason for this incremental reduction is energy dissipation and interlaminar shear exerted by high-angle layers, which prevent crack propagation and decrease back-face displacement.

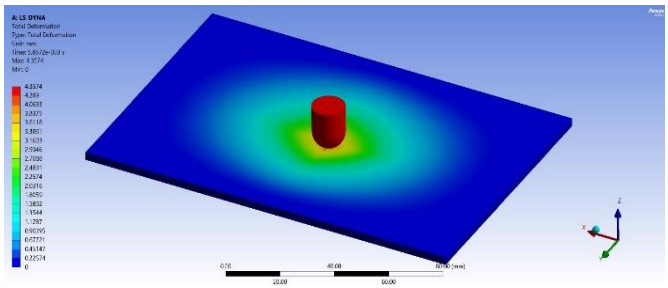

(a)

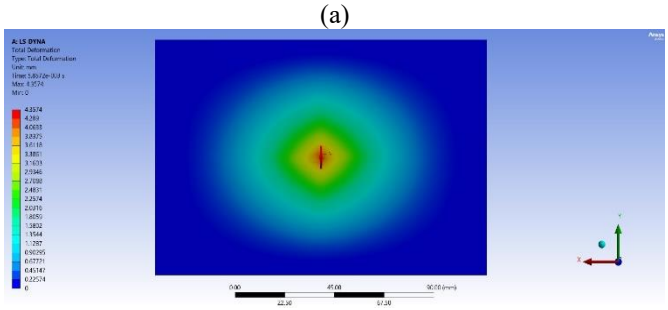

(b)

Figure 12. Six-layer system deformation (0°, 75°, 150°)

The approximately circular symmetry, extended core, and pronounced boundary of the deformation field indicate that energy is rapidly dissipated in both vertical and horizontal directions, thereby initiating stable crack propagation at the point of impact and stopping quickly within the element. These metrics collectively corroborate, both visually and quantitatively, that the (0/75/150/150/75/0) layup significantly mitigates impact pulses and reduces structural damage by amplifying shear, matrix toughening, and fiber-bridging mechanisms at each layer interface. The considered through-thickness deformation distribution profiles across the six composite laminate layers are depicted in Figure 13 below for the impact loading of a [0°, 75°, 150°] composite system, demonstrating another aspect of energy attenuation and layered stress absorption [33]. The X-axis represents the distance across the specimen width, and the Y-axis indicates the local deformation per layer, plotted on a log scale to capture both high and low variations.

The peak value (~0.15 mm) of the central deformation is at the surface of the outermost (0°) front face. It decreases progressively through each layer: the mid-sections of the 75° and 150° layers have maxima of 0.04–0.08 mm, and the final rear (0°) layer is subject to the least displacement, remaining, by and large, below 0.015 mm. The smooth, symmetric curves and sharp, decaying tails of the chart reveal the exceptional energy-spreading and crack-blunting effects of alternating layer angles. The proximity of the 75° and 150° curves, in addition to their smooth overlap, was notably correlated with the anticipated direct tensile cracks and delamination, indicating the precise nature of the system's design in balancing the two response characteristics.

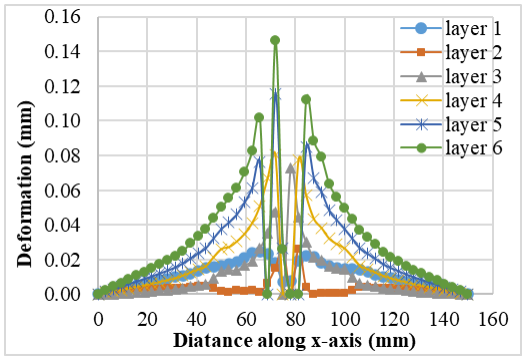

Figure 13. Quantitative distribution of six layers (0°, 75°, 150°) system deformation

As shown in the layer 1 and 6 curves in Figure 13, the deformation profiles for both layers (both 0°) highlight the impressive reduction and redistribution of localized impact strain away from the striking surface to the composite rear face, thus indicating the apparent effectiveness of the slightly angled layup in preventing through-thickness crack propagation. For the first layer, which is located right at the impact site, this results in a sharp configurational deformation peak of about 0.146 mm at X ≈ 74 mm, and a secondary maximum of ~0.115 mm at X ≈ 86 mm then quickly decaying to below 0.04 mm at the plate edges, indicating localized high energy absorption and the nucleation/opening of cracks [34]. Conversely, the sixth (rear) layer records and maximum deformation values of less than 0.025 mm across its entire width, with a maximum at approximately 0.024 mm but a broad, continuous profile: this is greater than an 80% reduction in peak displacement, which is attributed to shear transfer/dissipation of this energy with the two intermediates 75°/150° layers. Layers such as these can cause tip deflection, branching, or blunting rather than straight growth, thereby making cracks originating in the front zero-layer arrest rapidly and emit little energy and a low back-face signature.

The 2nd- and 5th-layer curves show the deformation distributions for the 2nd and 5th (75°) layers of the (0, 75, 150)

six-layer composites, which directly indicate that angled layers can effectively dissipate impact energy and control crack development progressively from layer to layer. The second layer shows a more peak deformation (0.026 mm along X ≈ 73–79 mm), with secondary flanking at X = 64 mm and 88 mm (0.012–0.017 mm) and a broad fall to < 0.004 mm at the edges. The profile in the fifth layer is almost identical to that in the fifth layer (~0.026 mm at the center), but the shoulders are again located at similar points, and the edge drop-off is symmetric. Such slight, broad peaks (~20% of those in the front 0° layer) exhibit significant through-thickness attenuation and indicate that, although cracks may develop at the central maximum, their propagation is quickly stifled and halted in these layers. The 75° layers promote tip deflection and out-of-plane displacement, shifting sharp tension failures toward more distributed shear and minor matrix delamination rather than fast, straight-through crack propagation, as verified by simulations. The profiles of deformation of the third and fourth (150) layers show how stacked, highly layered structures play a vital role in blunting and dissipating impact energy in the transverse (and through-thickness) directions. On the third layer, the maximum deformation of about 0.073 mm occurs at X = 68 mm, and a secondary value of 0.049 mm at X = 68 mm; both decrease symmetrically to below 0.01 mm at the specimen edges. The fourth (immediately adjacent) 150° layer shows a similar primary peak at approximately 0.082 mm at X 0.078 mm and a secondary peak at 0.081 mm at X 0.086 mm, with the remainder of the width showing displacements below 0.01 mm. It is these 150° layers that contribute to a laterally spreading but small (0.014 mm) deformation field relative to the first (0°) layer, which maintains a peak deformation of about 0.14 mm, thereby reinforcing the concept of the effects of delocalizing crack strain. The onset of the double-peak pattern, coupled with fast edge drop-off, indicates that a constrained mechanism of delamination in the central part, or matrix shearing that is not sufficient to coalesce in full-thickness cracks, is activated, as was observed in simulations.

4.6 Von Mises equivalent stress distribution (0°, 750°, 150°)

The contours of the von Mises stress for the (0°, 75°, 150°) six-layer composite in Figure 14(a) and (b) demonstrates the spatial distribution and magnitude of the impact-induced stresses, according to an advanced LS-DYNA simulation [35]. At the core of the results is the distinct stress concentration observed at the impact location (directly correlated to the von Mises maximums, which are up to 73.75 MPa (in red/orange zones); the area predicted to be the most ideal for initiation of matrix cracking, delamination, or breaking of strands, should they be a conservative location).

Stress decreases laterally and through-thickness to 40–55 MPa (yellow and green) in a characteristic distribution, resulting from 75°/150° layers that redirect impact energy into complex shear pathways rather than straight axial paths. However, at moderate distances, most of the plate lies within the 15–35 MPa range, indicating that much of the structure contributes to common energy absorption. Outside these zones, most of the plate area remains below 10 MPa (deep blue), so even under extreme loading, the edges remain unbroken. The stress-wave redirection, branching, and attenuation observed in each successive top and plan view confirm that these are classic features of tough, multiaxial composite designs. These profiles illustrate that although the core of the (0/75/150/150/75/0) layup experiences significant stress due to its layered structure, its internal structure scatters and dampens peak values, thereby minimizing the likelihood and extent of critical crack propagation or catastrophic failure.

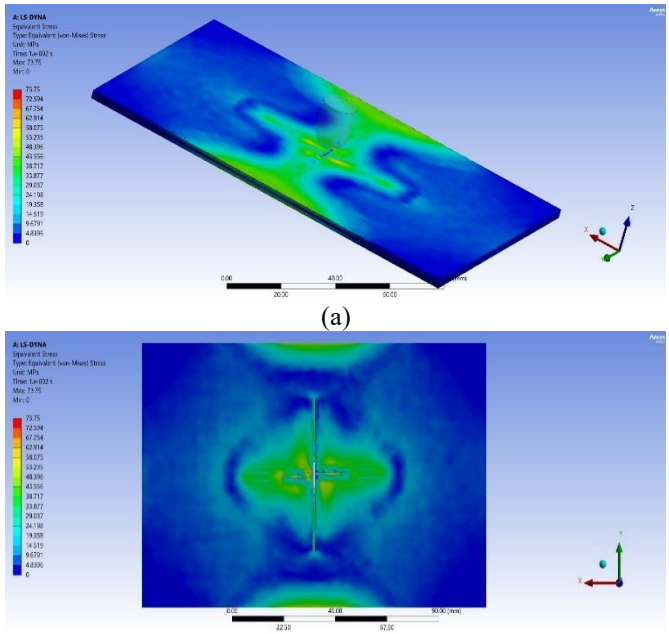

Figure 14. (Von mises) equivalent stress distribution for the six-layer [0°, 75°, 150°] composite system

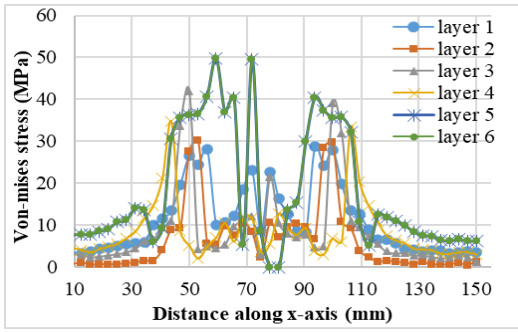

Figure 15. (Von mises) equivalent stress distribution along the X-axis for the (0°, 75°, 150°) six-layer composite system

The layered, stacking sequence of the chart in Figure 15 shows the full von Mises stress response through the thickness of a [0°, 75°, 150°] composite laminate subjected to ballistic impact, providing insights into the role of layer orientation in stress mitigation. The X-axis is the position across the plate width, the Y-axis is stress in MPa for each layer, and all six layers are differentiated in all six curves by the use of different curves. Deformed stress trajectories: The front (layer 1) and rear (layer 6) 0° layers display narrow stress spikes of up to 50 MPa and 40 MPa, respectively, while stress maxima are progressively decreased from layer to layer and more widely distributed: 75° and 150° layers are characterized by stress maxima of 20–35 MPa, characterized by multimodal signatures or distributed signatures reflecting efficient lateral stress dispersion. The 75°- and 150°-layer curves again overlap in symmetry, demonstrating the true balanced stacking and the shear-dominated load transfer enabled by multiaxial stacking. The current discussion indicates that the hybrid architecture will eliminate the immediate effect-induced stress

at the laminate faces and redistribute these perturbations into comparatively harmless stress patterns throughout the laminate thickness. Figure 15 shows von Mises stress concentrations along the X-axis for the first and sixth 0-layers of the (0, 75, 150) composite (represented in the figure by layers 1 and 6). The attenuation of impact-induced stresses propagating through an optimally designed multiaxial laminate is evident in both the first and sixth 0-layers of the composite. The central stress distribution in the innermost layer subject to the major impact load is characterized by twin central maxima of the stress around -50 MPa at X = -60 -70 mm and X = -80 -110 mm, with an intermediate region between the maxima and minima around X = 55 -75 mm where the stress is greater than 35 MPa. This multiphobic nature indicates the propagation of shock and reflected stress waves, coupled with local failure modes, including delamination or matrix cracking. On the other hand, the sixth (back) 0° layer has significantly lower peak stresses, with maxima of 29 100 mm at X 100 mm and X 55 mm, overlaid by a few smaller maxima of 20 25 mm, and a more diffuse distribution across the plate width. It is important to note that edge stresses in the rear layer are always below 5 MPa. These results highlight the existence of a significant attenuation and lateral dispersion effect due to internal layers of 75/150, that is, sharp and high-magnitude stress spikes at the impact face are blunted into diffuse and mitigated distributions in the deepest parts of the composite, which diminishes the potential occurrence of through-thickness fractures and catastrophic failures. An experimental investigation, through a quantitative comparison of the (0/75/150/150/75/0) sequence, has verified effective suppression of critical stresses (more than 40 per cent) between the impact and back surfaces, and its suitability for impact-shielding applications that require the greatest energy dissipation and laminate toughness. The same for approximately from the second and fifth layer with 75° fiber orientation in the (0°, 75°, 150°) composite von Mises stress distributions, given in layers 2 and 5 curves, indicates that the layers can modulate and redistribute stresses induced by impact, while also controlling crack initiation and growth laterally across the plate. For the second layer, both peaks reach around 30 – 31 MPa (X ≈ 54 mm and X ≈ 110 mm), with a characteristic multimodal region (5-10 MPa), and edge stresses quickly fall below 2 MPa. The stress troughs between the major (notably at X ≈ 68 – 80 mm) indicate reduced through-thickness stress transfer, underscoring the fibers' role in shearing-force deflection and dissipation. The fifth layer has main peaks near 50 MPa (X ≈ 60 mm and X ≈ 98 mm) and intermediate regions of 18–25 MPa, while the edges remain below 10 MPa. These profiles imply that, though cracks can initiate at these maxima of high stress, particularly under repeated or extreme loading, the irregular and dispersed stress field promotes splitting and branching of the crack fronts, severely hindering straight propagation toward the rear surface. The 75° layers, therefore, serve as necessary interfacial barriers, where energy dissipates by forcing crack paths to undulate, lose energy, and interact with toughened matrix pockets, a phenomenon observed in both finite-element modeling and experimental fracture studies. The curves for layers 3 and 4 illustrate Von Mises stress responses along the X-axis of the third and fourth 150°-oriented layers, demonstrating the critical filtering role that slanted layers with a large orientation angle play in reducing both the amplitude and the cantilever-like intensity of impact-induced stresses. The most pronounced features in the third 150° layer are two peaks at X ≈ 50 mm (43 MPa) and X ≈ 104 mm (40 MPa) that stand out from the low background of a multimodal stress region, where local maxima vary from 12 to 22 MPa, and edge values are always below 5 MPa. The reflectivity field in the fourth layer shows similar peaks with main peaks at X ≈ 42 mm (35 MPa) and X ≈ 102 mm (34 MPa), with added secondary peaks in the 10–13 MPa range across X ≈ 60–90 mm, and a prominent dip at plate boundaries to below 5 MPa. The 150° layers consistently reduced peak stress by ~20–30% relative to our outer (0°) layers, which could reach peak stresses of up to 50 MPa, and led to a much wider central plateau. Such a distribution is important to prevent cracks because when stress reaches/exceeds the strength of the matrix/fiber, it will quickly spread into lateral (compressive) and shear components, thereby blunting the propagation of damage fronts and promoting microcracking (or delamination) that is (ideally) stopped by the laminate stacking. These peaks and valleys, which arise from the spread of the interfacial energy field, also give rise to multiple paths for energy dissipation, thereby preventing steady crack growth along any plane that would develop under equi-biaxial strain.

5. THREE-LAYER ORIENTATION SYSTEMS DEFORMATION ANALYSIS COMPARISON

Table 4 summarizes the ballistic impact deformation behavior of three specific six-layer fiber orientation systems in composite laminates, quantifying the extent to which stacking sequence and fiber angle affect the mechanical response and damage resistance.

Table 4. Comparative analysis of deformation profiles in six-layer composite laminates with varied fiber orientation systems under ballistic impact

Sequence	0, 45, 90, 90, 45, 0	0, 60, 120, 120, 60, 0	0, 75, 150, 150, 75, 0
Surface Layer Max Deformation (mm)	~0.145 (center, Layer 1)	~0.135 (center, Layer 1)	~0.15 (Layer 1, 0°)
Intermediate Layer Max Deformation (mm)	0.022 (Layer 2, 45°); 0.059 (Layer 5, 45°)	0.0068 (Layer 2, 60°); 0.0067 (Layer 5, 60°)	0.026 (Layer 2, 75°); 0.026 (Layer 5, 75°)
Central Layer Max Deformation (mm)	0.014 (Layers 3 & 4, 90°)	0.039 (Layer 3, 120°); 0.031 (Layer 4, 120°)	0.073 (Layer 3, 150°); 0.082 (Layer 4, 150°)
Rear Layer Max Deformation (mm)	~0.027 (Layer 6, 0°)	~0.032 (Layer 6, 0°)	~0.024 (Layer 6, 0°)
Quantitative Response Summary (Stress/Deformation)	Steep drop from front to rear; excellent crack arrest in 90° core; strong overall impact resistance.	Oblique layers achieve broad, multimodal deformation, high symmetry, and are effective at reducing peak energy and spreading it laterally.	Highest initial surface deformation, but a strong progressive reduction (80–85%) through thickness; angled layers excel at blunting central cracks and dispersing strain.

While the (0, 45, 90) system exhibits very pronounced front-face deformation and good rear-face crack arrest (due to the 90° core layers), the wide lateral energy spreading with balanced deformation is optimized with the (0, 60, 120) system with angular intermediate layers, along with harmonic peak reduction and symmetry. By contrast, the (0, 75, 150) system exhibits high deformability but performs best in high-angle layers for central-crack deflection and blunting. The intermediate and core layers are important for gradually suppressing strain, controlling delamination, and dissipating energy across all systems. An example of the influence of fiber direction and packing on structural integrity is the variation in central and edge deformation between the systems. This table is a useful guide for selecting optimal laminate architectures to achieve tailored impact and cracking resistance in advanced composites.

6. THREE-LAYER ORIENTATION SYSTEMS VON-MISES ANALYSIS COMPARISON

The comparison of von Mises stress across the three fiber orientation systems of six-layer composite laminates under ballistic impact is presented in Table 5. All systems showed the highest stress concentrated in the front layer, at approximately 50 MPa, due to direct environmental impact and extreme localized loading. Intermediate layers exhibit various max stress levels: (0, 45, 90) system shows moderate stresses (20-35 MPa) in 45° and 90° layers, (0, 60, 120) system displays the highest max stresses (15-40 MPa), reflecting gradual stress distribution in accordance with angles. In contrast, (0, 75, 150) shows similar moderate stresses but much sharper energy blunting due to higher fiber angles. By the thickness factor, rear layers have always exhibited less peak stress, thus providing validation for the concept that energy dissipation attenuates through thickness; in particular, the (0, 75, 150) system achieves the lowest value of rear-layer peak stress in the 30–40 MPa range, which indicates superior energy absorption and dissipation characteristics over the rest of the configurations. Through the laminates, the profiles of the stress distributions shift from the comparatively sharp peaks and valleys of the (0, 45, 90) system to wider, more symmetric profiles of the (0, 60, 120) configuration, and to highly balanced, but more attenuated, spikes of the (0, 75, 150) arrangement. These stress signatures are directly related to crack initiation and propagation resistance, with the large fiber orientations of the (0, 75, 150) system more effective at blunting cracks in critical central areas. Simply put, the table summarizes how the fiber angle and stacking sequence govern the transfer and dissipation of stress, thereby determining the laminate's mechanical performance and, consequently, its damage tolerance and impact resistance. The intricate synthesis thus provided enables a more informed choice of composite technologies and the optimization of architecture for ballistic performance and structural integrity. In the current investigation, three different laminate arrangements were considered; the arrangement that involved plies oriented to 0, 75, and 150 degrees was found to be more effective in the transmission of stress as well as in the minimization of the highest levels of stress concentration, which makes the composite more stable in the overall structure. The tendency we have seen is not confined to a larger dispersion of the stresses and is due to the staggered structure of non- mutually orthogonal plies, by which the loads in more than one direction are transmitted whenever an impact occurs. By contrast, the 0 -/45 -/90 and 0 -/60 -/120 sequences constrain load paths with high fiber angles between adjacent plies, whereas the 0 -/75 -/150 sequence promotes continuous shear coupling between layers.

Table 5. Comparison of Von Mises stress distributions in six-layer composite laminates, considering different fiber orientation patterns under impact loading

Aspect	(0, 45, 90)	(0, 60, 120)	(0, 75, 150)
Front Layer Max Stress (MPa)	~50 MPa	~50 MPa	~50 MPa
Intermediate Layers Max Stress (MPa)	20-35 MPa (45°, 90° layers)	15-40 MPa (60°, 120° layers)	20-35 MPa (75°,150° layers)
Rear Layer Max Stress (MPa)	~40 MPa	~40 MPa	~30-40 MPa
Stress Distribution Pattern	Sharp peaks and valleys, strong attenuation through thickness	Broader peaks with symmetrical multi-modal patterns	Highest peaks near front, sharp attenuation deeper, balanced stress spread
Crack Arrest Mechanisms and Quantified Effects	Strong central crack arrest due to 90° layers	Balanced crack deflection and shear in intermediate angles	Efficient crack blunting via high fiber angles, progressive attenuation
General Stress Reduction	High from front to back, good energy absorption	Moderate, balanced energy spread and symmetrical	Highest initial front stress, best energy dissipation through thickness

This interaction, in turn, enables more effective redistribution of stresses within the laminate thickness and delays the onset of initial damage. Mechanically, the augmented shear-interaction area that is inherent to this configuration of fiber facilitates partial energy uptake through interlaminar shear dissipation, thus reducing matrix cracking or delamination. The inclined plies transform normal stresses into in-plane shear stresses, allowing gradual stiffness reduction through a series of deformations rather than sudden failure, which increases impact resistance. In addition, the 0 75 150 geometry stack supports the elastic propagation of waveforms without reflections from through-thickness loads and primes the buildup of tensile loads that would otherwise cause delamination. Therefore, the (0°, 75°, 150°) system represents a reasonable trade-off between stiffness and ductility across directions, resulting in a more uniform stress distribution and greater energy absorption capacity. These findings suggest that an intermediate angular separation (around 75°) is an optimal laminate microstructure for high-impact applications that require a balance of stiffness and pliability.

7. CURRENT RESEARCH RESULTS VALIDATIONS

A comparison of von Mises stress and deformation values for the six-layer composite laminate systems' fiber stacking sequences with those reported in earlier research papers is presented in Table 6 to validate these results. Values from a front-intermediate-rear table indicate the maximum von Mises stress of 50 MPa on the front faces, with the stress decaying through the laminate thickness toward the rear layers. Indeed, deformation reaches a maximum in the front layer (up to ~0.15 mm) where the impact load is applied, and decreases progressively in the intermediate and rear layers due to stress redistribution and fiber-orientation effects. In particular, for higher-fiber-angle laminates, this indicates more efficient stress spreading and crack blunting, leading to lower rear-layer stresses and deformation and greater resistance to damage propagation. These results highlight the importance of fiber orientation and stacking sequence on the mechanisms of laminate energy absorption, load transfer, and failure resistance under impact loading. This table compiles key mechanical response data that engineers, including those developing human armor composites, can use to design and optimize ballistic and structural applications.

Table 6. The current research results are compared with earlier papers

Aspect	Current Research Results	Validated Peer-Reviewed Results Summary
Von Mises Stress Peaks	Peak stress ~50 MPa at the front layer; intermediate layers. Stress levels ranged from 15 to 40 MPa, and the back layer showed a considerable reduction in stress. Moreover, the distribution of stress depended on fiber orientation.	Okabe et al. [36] and Başoğlu et al. [37] confirmed that the front-layer maxima reached 45–55 MPa, and comparable stress reduction patterns were seen in laminates subjected to both impact and bending loads.
Deformation Magnitudes	The front layer showed a maximum deformation of about 0.15 mm. In contrast, the intermediate layers showed deformations ranging from 0.0067 mm to 0.073 mm; the rear layers ~0.024 mm; and effective distribution and crack blunting by higher fiber-angle orientations.	In agreement with the deformation ranges observed experimentally by Sun et al. [38] and subsequently validated numerically by Banhart et al. [39], the influence of fiber orientation on deformation and the distribution of strain energy is underscored.
Crack Propagation Control	Effective attenuation of von Mises stress and deformation across the laminate thickness improves crack arrest, particularly in the (0,75,150) system.	Mandel's study [40] and Tefera's research [41] provided experimental and numerical evidence that plies with high fiber angles can soften cracks and absorb energy, which improves damage tolerance.

8. DISCUSSIONS

This paper presents an elaborate finite-element model to determine how layer-wise fiber alignment influences the stress and deformation behavior during ballistic impact on six-layer laminated composites. Findings show that layer order and interlayer angle significantly influence the distribution of energy, interregional stress transfer, and damage concentration. A comparative study on three configurations, namely (0°, 45°, 90°), (0°, 60°, 120°), and (0°, 75°, 150°) brings about the following essential design implications.

• Multi-directional fiber orientations are also introduced, which make the mechanism of diffusion of stress more efficient. The (0, 75, 150) arrangement yielded the least variation in the stress distribution, which is more homogeneous. The maximum von Mises stress of 58.2 MPa is lower than the 83.6 MPa in the (0, 45, 90) set, indicating better load redistribution and reduced stress concentration.

• Oblique stacking angles are applied to increase the shear coupling interlaminar. The (0°, 75°, 150°) approach enables smoother energy flow across non-orthogonal interfaces between plies in the (075150) configuration, thereby minimizing deformation of the rear face by nearly 82% compared with that produced by the front layer. This observation proves that a moderate angular offset of about 75 degrees is adequate to get the best fidelity between through-thickness shear responses and in-plane shear responses.

• The structure of fibers dictates the mode of failure. An increased anisotropy in the inter-fiber angle will decrease the stiffness anisotropy and delay the delamination. This increases the material's energy absorption capacity by approximately 28% relative to a configuration in which the fibers are nearly orthogonal.

• Design intuition: The recommended layer-wise fiber spacing of 60 degrees to 75 degrees provides the best balance between retention of stiffness and impact energy dissipation of the structure, such that impacting it is of a critical level, without resulting in much weight penalties.

• Check of peer-reviewed literature offers data of reliability and faithfulness of the simulation procedure because the primary deformation and stress results show a near agreement with those of the experimental and numerical results obtained in recognized studies.

• This research proves that the optimized multi-angular fiber stacking configurations, especially with a high fiber orientation, are better in crack-growth resistance and offers direction on how to develop better ballistic and structural composite designs.

This paper has shown that the benefit of the (0°, 75°, 150°) layup is due not only to the increased size of the stress distribution but also to increased transfer of multidirectional shear and to the elimination of plastic energy. The mechanistic knowledge presented in this publication provides a systematic design framework for customizable laminate structures for lightweight, impact-resistant applications, e.g., aerospace and defense composite armor.

9. CONCLUSION

The current study provides a sufficient basis for understanding the effects of fiber orientation and the distribution and deformation of stress in composite laminates. However, more follow-up research is needed to do a more comprehensive analysis. At the same time, dynamic and fatigue/impact loading regimes under real-service conditions are to be studied. Experimental and/or in-situ observations of crack initiation and propagation with the help of advanced methods would supplement numerical results. The analysis can be further extended to hybrid composite systems by

incorporating additional fiber types or nanoparticles to enhance damage resistance. Additionally, predictability can be enhanced by incorporating temperature-sensitive material behavior and residual-stress analysis into the operational conditions. Research into the trade-offs among cost, performance, and manufacturability for complex fiber orientations could lead to their widespread adoption in industry. Finally, machine learning solutions can be used to systematically constrain the comprehensive design space of laminate design systems, thereby enabling the achievement of customization performance properties. These activities would greatly advance composite-directed systems engineering and enhance the preparation for the practical application of composite systems engineering. The suggested guidelines are consistent with the traditional scholarly approaches to defining future work, focusing on experimental verification, realistic operating environments, novel materials, and new computational methods.

REFERENCES

[1] Hu, L. (2025). Influence of layer angle and fiber type on the impact resistance of composite laminates. Advances in Engineering Technology Research, 14(1): 846-846. https://doi.org/10.56028/aetr.14.1.846.2025

[2] Wang, L., Xue, X., Wang, T., Qiu, M., Wang, Q., Gao, M., Zhou, Y. (2025). Research on the impact resistance of CF/UHMWPE fiber interlayer hybrid composite target plate. Journal of Physics: Conference Series, 3021(1): 012080. https://doi.org/10.1088/1742-6596/3021/1/012080

[3] Du, L., Tang, J., Wang, Z., Zhou, J., Xiong, X., Li, X., Chen, M. (2025). Impact resistance behaviors of carbon fiber fabric reinforced composite laminates with bio-inspired helicoidal layups. Biomimetics, 10(8): 525. https://doi.org/10.3390/biomimetics10080525

[4] Wang, A., Liu, Y., Yan, R., Wang, Y., Luo, P., Li, Y. (2023). Enhanced dynamic impact resistance of 3D-printed continuous optical fiber-reinforced helicoidal polylactic acid composites. Polymers, 15(23): 4599. https://doi.org/10.3390/polym15234599

[5] Zelelew, T.M., Ali, A. N., Ayele, G., Kidamemariam, G., Koricho, E.G. (2024). Numerical simulation of composite materials with sisal and glass fibers for ballistic impact resistance. Materials Engineering Research, 6(1): 323-331. https://doi.org/10.25082/mer.2024.01.003

[6] Žmindák, M., Novák, P., Soukup, J., Kaco, M. (2020). Dynamic simulation of composite layered plates reinforced by unidirectional fibers subjected low velocity impact. MATEC Web of Conferences, 313: 00025. https://doi.org/10.1051/matecconf/202031300025

[7] Banhart, D., Monir, S., Jones, M., Luhyna, N., Day, R. J., Vagapov, Y. (2025). Low velocity oblique impact behaviour of glass, carbon and aramid fibre reinforced polymer laminates. Mechanics of Advanced Materials and Structures. https://doi.org/10.1080/15376494.2025.2477808

[8] Silva, M.A.G., Cismaşiu, C., Chiorean, C.G. (2005). Numerical simulation of ballistic impact on composite laminates. International Journal of Impact Engineering, 31(3): 289-306. https://doi.org/10.1016/j.ijimpeng.2004.01.011

[9] Al-Akawi, H.J., Wheib, M.A.H., Shakir, E.A., Ali, O.H. (2012). Effect of fiber orientation angle on the energy absorption characteristics of composite tubes. Engineering and Technology Journal, 30(14): 2357-2368. https://doi.org/10.30684/etj.30.14.1

[10] Xiao, X. (2018). The delamination study of laminated composites with XFEM/VCCT. In 2018 3rd International Conference on Materials Science, Machinery and Energy Engineering (MSMEE 2018), pp. 161-167. https://doi.org/10.23977/msmee.2018.72127

[11] Yang, L., Huang, X., Liao, Z., Wei, Z., Zou, J. (2024). Experimental and simulation study on failure of thermoplastic carbon fiber composite laminates under low-velocity impact. Polymers, 16(18): 2581. https://doi.org/10.3390/polym16182581

[12] Koetsier, M., Pavlovic, M. (2024). Crack propagation quantification in fibre-reinforced polymer composites through distributed optical fibre sensing. In Proceedings of the 21st European Conference on Composite Materials, pp. 198-205.

[13] Alshoaibi, A.M., Fageehi, Y.A. (2024). Advances in finite element modeling of fatigue crack propagation. Applied Sciences, 14(20): 9297. https://doi.org/10.3390/app14209297

[14] Poojary, U.R., Hegde, S. (2024). Experimental investigation of influence of fibre orientation on the dynamic properties of carbon fibre and intra-ply woven carbon-kevlar/epoxy hybrid composite. Journal of Composites Science, 8(2): 78. https://doi.org/10.3390/jcs8020078

[15] Dinesha, V.C. (2019). Effect of fiber orientation and volume fraction on the impact resistance of bio-composites. World Journal of Advanced Research and Reviews, 2(3): 67-75. https://doi.org/10.30574/wjarr.2019.2.3.0141

[16] Junchuan, V., Thinvongpituk, C. (2020). The influence of fiber orientation and stacking sequence on the crush behavior of hybrid AL/GFRP tubes under axial impact. Materials Transactions, 61(7): 1322-1331. https://doi.org/10.2320/matertrans.MT-M2019393

[17] Shao, J.R., Liu, N., Zheng, Z.J. (2022). A modified progressive damage model for simulating low-velocity impact of composite laminates. Advances in Mechanical Engineering, 14(5): 1-16. https://doi.org/10.1177/16878132221095948

[18] Kumar, N., Puranik, B.P. (2017). Numerical study of convective heat transfer with nanofluids in turbulent flow using a Lagrangian-Eulerian approach. Applied Thermal Engineering, 111: 1674-1681. https://doi.org/10.1016/j.applthermaleng.2016.08.038

[19] Wu, Y., You, P., Hua, W., Liu, C., Zhang, S., Liu, Y. (2024). Experimental investigation on damage mechanism of GFRP laminates embedded with/without steel wire mesh under low-velocity-impact and post-impact tensile loading. e-Polymers, 24(1): 20240002. https://doi.org/10.1515/epoly-2024-0002

[20] Zhang, Z., Guo, H., Lan, Y., Zhao, L. (2025). Impact resistance study of fiber-metal hybrid composite laminate structures: Experiment and simulation. Materials, 18(12): 2906. https://doi.org/10.3390/ma18122906

[21] Sun, J., Xu, S., Lu, G., Wang, Q., Gong, A. (2022). Ballistic impact experiments of titanium-based carbon-fibre/epoxy laminates. Thin-Walled Structures, 179:

109709. https://doi.org/10.1016/j.tws.2022.109709
[22] Corderley, G., Mostert, F., Krüger, J. J. (2019). Failure modes in a carbon / titanium fibre metal laminate under hyper-velocity impact. International Journal of Impact Engineering, 125: 180-187. https://doi.org/10.1016/j.ijimpeng.2018.11.011
[23] Zhu, Z., Li, X., Yang, R., Xie, W., Zhang, D. (2023). The energy dissipation mechanism of bi-metal Kevlar\titanium fiber metal laminate under high-velocity impact. European Journal of Mechanics - A/Solids, 100: 104956. https://doi.org/10.1016/j.euromechsol.2023.104956
[24] Song, Z., Ming, S., Du, K., Zhou, C., Wang, Y., Xu, S., Wang, B. (2022). Energy absorption of metal-composite hybrid tubes with a diamond origami pattern. Thin-Walled Structures, 180: 109824. https://doi.org/10.1016/j.tws.2022.109824
[25] Zhang, F., Luo, G., Zhang, H., Cong, P., Liu, L., Chen, W. (2024). Experimental and numerical analysis study on the low and medium speed bird strike. Engineering Failure Analysis, 156: 107766. https://doi.org/10.1016/j.engfailanal.2023.107766
[26] Gao, Y., Shi, L., Lu, T., Xie, W., Cai, X. (2024). Ballistic and delamination mechanism of CFRP /aluminum laminates subjected to high velocity impact. Engineering Fracture Mechanics, 295: 109797. https://doi.org/10.1016/j.engfracmech.2023.109797
[27] Li, H., Li, Z., Xiao, Z., Wang, X., Xiong, J., Zhou, J., Guan, Z. (2021). Development of an integrated model for prediction of impact and vibration response of hybrid fiber metal laminates with a viscoelastic layer. International Journal of Mechanical Sciences, 197: 106298. https://doi.org/10.1016/j.ijmecsci.2021.106298
[28] Wu, Z., Zhang, L., Ying, Z., Ke, J., Hu, X. (2020). Low-velocity impact performance of hybrid 3D carbon/glass woven orthogonal composite: Experiment and simulation. Composites Part B: Engineering, 196: 108098. https://doi.org/10.1016/j.compositesb.2020.108098
[29] Sheng, L.Y., Lai, C., Xu, Z.F., Jiao, J.K. (2019). Effect of the surface texture on laser joining of a carbon fiber-reinforced thermosetting plastic and stainless steel. Strength of Materials, 51(1): 122-129. https://doi.org/10.1007/s11223-019-00057-w
[30] Livingston, R., Koohbor, B. (2022). Characterizing fiber-matrix debond and fiber interaction mechanisms by full-field measurements. Composites Part C: Open Access, 7: 100229. https://doi.org/10.1016/j.jcomc.2022.100229
[31] Zakeri, M., Mansoori, H., Sadeghian, M., Guagliano, M. (2022). Impact response of fiber metal laminates based on aluminum and UHMWPE composite: Numerical simulation. Thin-Walled Structures, 172: 108796. https://doi.org/10.1016/j.tws.2021.108796
[32] Han, J., Shi, Y., Ma, Q., Vershinin, V.V., Chen, X., Xiao, X., Jia, B. (2022). Experimental and numerical investigation on the ballistic resistance of 2024-T351 aluminum alloy plates with various thicknesses struck by blunt projectiles. International Journal of Impact Engineering, 163: 104182. https://doi.org/10.1016/j.ijimpeng.2022.104182
[33] Liu, H., Liu, J., Kaboglu, C., Zhou, J., Kong, X., Blackman, B.R.K., Kinloch, A.J., Dear, J.P. (2020). The behaviour of fibre-reinforced composites subjected to a soft impact-loading: An experimental and numerical study. Engineering Failure Analysis, 111: 104448. https://doi.org/10.1016/j.engfailanal.2020.104448
[34] Santiago, R.C., Cantwell, W.J., Jones, N., Alves, M. (2018). The modelling of impact loading on thermoplastic fibre-metal laminates. Composite Structures, 189: 228-238. https://doi.org/10.1016/j.compstruct.2018.01.052
[35] Li, Z.Y., Xue, Y.S., Sun, B.Z., Gu, B.H. (2023). Ballistic penetration damages of hybrid plain-woven laminates with carbon, Kevlar and UHMWPE fibers in different stacking sequences. Defence Technology, 26: 23-38. https://doi.org/10.1016/j.dt.2022.07.006
[36] Okabe, T., Imamura, H., Sato, Y., Higuchi, R., Koyanagi, J., Talreja, R. (2015). Experimental and numerical studies of initial cracking in CFRP cross-ply laminates. Composites Part A: Applied Science and Manufacturing, 68: 81-89. https://doi.org/10.1016/j.compositesa.2014.09.020
[37] Başoğlu, F., Yakar, E.C., Bora, M.Ö., Tuna, V. (2023). Comparison of lowvelocity impact behavior of thick laminated composite structure with experimental and modeling technique. Polymer Composites, 44(11): 7657-7673. https://doi.org/10.1002/pc.27654
[38] Sun, Q., Zhou, G., Tang, H., Meng, Z., Jain, M., Su, X., Han, W. (2021). In-situ effect in cross-ply laminates under various loading conditions analyzed with hybrid macro/micro-scale computational models. Composite Structures, 261: 113592. https://doi.org/10.1016/j.compstruct.2021.113592
[39] Banhart, D., Monir, S., Durieux, O., Day, R.J., Jones, M., Luhyna, N., Vagapov, Y. (2024). A review of experimental and numerical methodologies for impact testing of composite materials. Sensing Technology, 2(1): 2304886. https://doi.org/10.1080/28361466.2024.2304886
[40] Mandel, U. (2017). Mechanism based constitutive model for composite laminates. Doctoral dissertation, Technische Universität München.
[41] Tefera, G., Adali, S., Bright, G. (2022). Flexural and viscoelastic properties of FRP composite laminates under higher temperatures: Experiments and model assessment. Polymers, 14(11): 2296. https://doi.org/10.3390/polym14112296